Royal Meteorological Institute of Belgium

Hail detection using radar observations: case studies in the summer 2002

L. Delobbe, D. Dehenauw, K. Hamid, and J. Neméghaire

2003

Wetenschappelijke en
technische publicatie
N^{r} 029

Uitgegeven door het
KONINKLIJK METEOROLOGISCH INSTITUUT VAN BELGIE
Ringlaan 3, B-1180 Brussel
Verantwoordelijke uitgever: Dr. H. Malcorps

Publication scientifique
et technique
N^{r} 029

Edité par
l'INSTITUT ROYAL METEOROLOGIQUE DE BELGIQUE
Avenue Circulaire 3, B-1180 Bruxelles
Editeur responsable: Dr. H. Malcorps

Table of Content

1 Introduction

Hail is regularly observed in Belgium and is sometimes the cause of severe damage on e.g. crops, greenhouses, roofs and cars. Most severe hail events occur in summer and are associated with intense thunderstorms producing large hail stones. Hail is a very local phenomenon, in time and space, which can not be easily detected with ground observational networks. Due to its wide spatial coverage and relatively fine spatial and time resolution, weather radar appears as a valuable tool for the real-time detection of hail.

Since November 2001, the Royal Meteorological Institute of Belgium has been operating a new weather radar in Wideumont, in the South of Belgium, near the borders with France and Luxembourg. The radar is a Gematronik C-band Doppler radar. It performs a standard scan with 5 elevation angles every 5 minutes allowing detection of precipitation up to a maximum range of 240 km (Fig. 1.1). In addition, a volumic scan including 10 elevations is performed every 15 minutes giving a three dimensional view op precipitation in the atmosphere. Volumic radar data allows estimating the vertical extension of thunderstorm cells. This is of great interest for hail detection purpose since the severity of a thunderstorm is strongly related to its vertical extension.

Various methods for the detection of hail from radar data have been proposed in the literature. In the framework of the present study, one of these methods has been selected and tested on different hail cases observed in Belgium in the summer of 2002. The aim is to evaluate the performance of the hail detection algorithm. The collected hail reports gave us also the opportunity to analyse different hail episodes that occurred in Belgium during that summer. For each selected case, the meteorological situation was analysed, radar data were compared with data from the lightning detection system SAFIR, and the performances of two atmospheric mesoscale prediction models in use at RMI were evaluated.

This report is organised as follows. In the next section, atmospheric processes involved in the formation of hail are shortly described and the currently used methods for radar-based hail detection are presented and discussed. Based on this discussion, one method will be selected for further testing. In section 3, the inventory of the reported hail cases in the summer 2002 is given and the meteorological situation associated with the hail episodes is analysed. The implementation of the selected hail detection method is described in section 4 and the results obtained for the different hail cases are presented and evaluated. Comparisons between reflectivity data from the weather radar and the electrical activity observed by the SAFIR system are shown in section 5 and the results obtained with two mesoscale prediction models are presented in section 6. Finally, the main results of this study are summarized and conclusions are drawn.

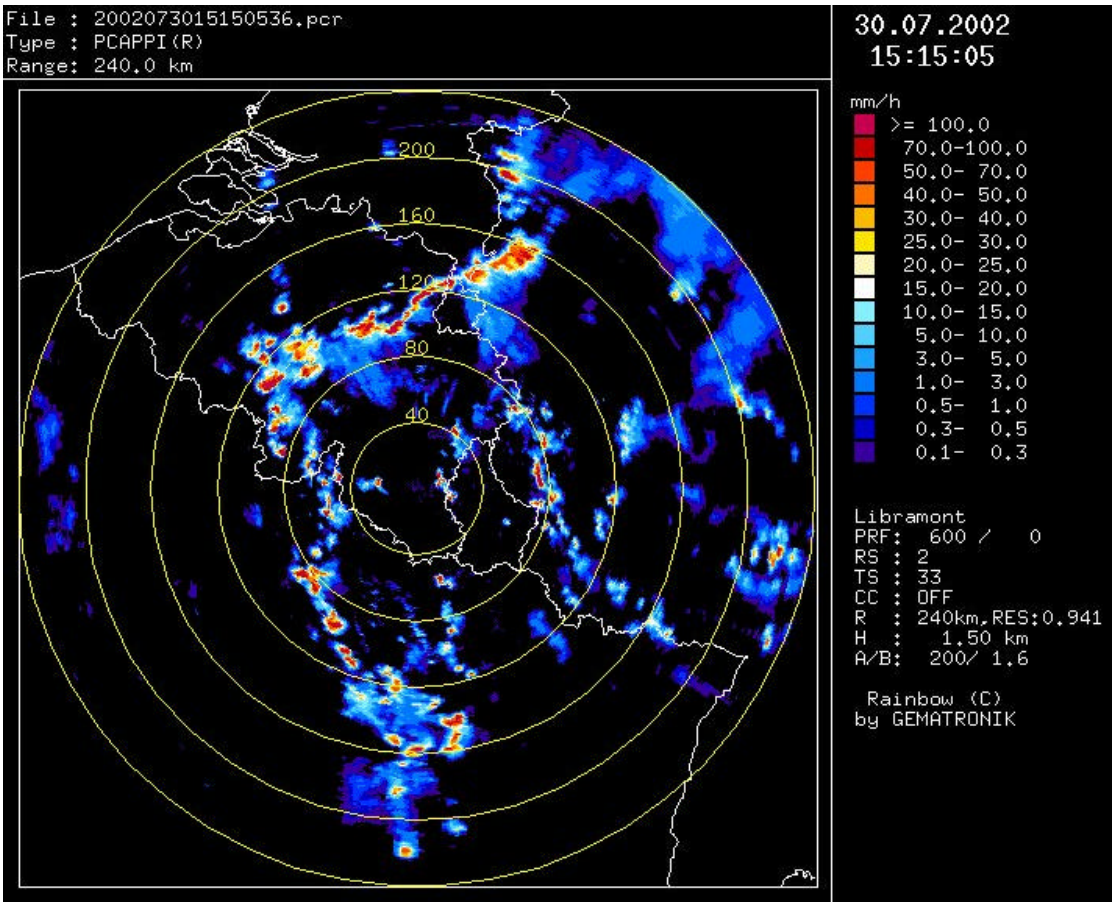

Figure 1.1: Precipitation image from the radar of Wideumont for the thunderstorm situation of July 30, 2002. Precipitation rates are derived from the reflectivity data collected by the radar.

2 Radar-based hail detection

2.1 Hail development processes

The microphysical processes responsible for hail development are not yet completely understood. Ice particles may form in a cloud if the temperature drops below zero. However, the transformation to ice does not take place readily and the ice phase becomes frequently observed only as cloud temperatures approach –20°C (Pruppacher and Klett, 1997). Liquid water that is colder than 0°C is called supercooled. At temperatures below 0 °C, the coexistence of supercooled water drops and ice particles is an important factor for the development of hail stones. Three different mechanisms are responsible for the growth of ice particles.

The first mechanism is the collision and aggregation of ice particles. This mechanism is often referred to as clumping and is mainly active at the initial stage of the particle growth. The second mechanism is the deposition, i.e. water vapor diffusion to the ice particles. The presence of liquid water ensures the diffusional growth of the ice crystals at the expense of water drops through the Bergeron process (Bergeron, 1933). This process relies primarily on the fact that the saturation vapor pressure with respect to ice is less than the saturation vapor pressure with respect to water. The last mechanism is the riming, i.e. the collection and freezing of water droplets colliding with ice particles.

The initial growth of ice crystals is primarily through clumping and vapor deposition until they are large enough to begin riming (Jameson and Johnson, 1990). When riming of an ice particle has proceeded to the stage where the features of the original ice crystal are no longer visible, the ice particle is referred to as a graupel. Rimed particles that have reached a diameter larger than 5 mm are called hailstones.

The production of large hailstones needs a rapid growth of ice particles through the above-mentioned mechanisms. Favorable conditions are found in intense thunderstorms where water and ice coexist in the central updraft. There is a positive relationship between the apparent strength of a storm (strength and size of updraft) and the size of hail that it produces (Ray, 1990). Growth of hailstones is highly influenced by the flow dynamics within thunderstorm (Heymsfield et al., 1980; Nelson, 1983). The interactions between microphysical processes and thunderstorm flow fields are complex. Trajectories of hail stones depend on the type of storm. In supercell storms, it is thought that most hail mass is acquired during a single pass across the updraft (e.g., Browning and Foote, 1976). More complex trajectories can be found in multicells where hailstones may recirculate in different cells of the thunderstorm complex, resulting in successive growth cycles. Nelson (1983) concludes that the most critical storm feature for large hail to be produced is the presence of a broad area of moderate updraft ensuring a sufficient residence time in a favorable growth environment.

2.2 Radar-based hail detection methods

The most efficient technique for discrimating hail from water is given by dual polarization radars (e.g., Seliga et al., 1982). Reflectivities in horizontal (Z_H) and vertical polarizations (Z_V) are similar for spherical hailstones which is not the case for non-spherical rain drops. The widely used parameter in this technique is the differential reflectivity defined as :

$$Z_{DR} = 10 \log\left(\frac{Z_H}{Z_V}\right)$$

Very large reflectivities together with low values of differential reflectivity is the signature of hail precipitation.

Another technique for hail detection is the dual-wavelength algorithm that was first proposed by Atlas and Ludlam (1961). This method is based on the measurements from a dual wavelength radar and makes use of the reflectivity dependence on the wavelength which is much higher for hailstones than for water drops. This technique does not receive the same degree of attention as the dual polarization but some new developments have been recently published (Feral et al., 2003).

Most radars of the current operational networks are single wavelength and single polarization radars. Various methods have been proposed for detecting hail using reflectivity measurements from this type of radar. In this section, we give a short overview of the currently used methods. An extended review can be found in Holleman (2001).

The most straightforward way for detecting hail is based on the Pseudo Constant Altitude Plan-Position Indicator product (**Pseudo CAPPI**). This product is generated from a radar scan at multiple elevations. The Pseudo CAPPI represents the reflectivity values at a given altitude above mean sea level. It is produced by interpolating between the reflectivity data from the different elevations. At short ranges, where the highest radar beam is lower than the selected altitude, the reflectivity data are taken from the highest elevation. At long ranges, where the lowest beam is above the selected altitude, the data are taken from the lowest elevation. For the radar of Wideumont, the selected altitude is 1500 m and the Pseudo-CAPPI is generated every 5 minutes from a scan at 5 elevations (Fig. 2.1).

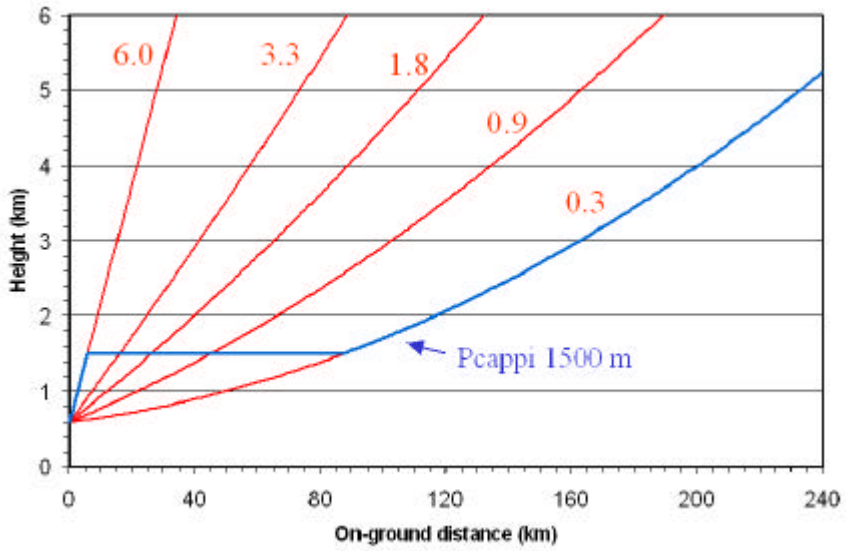

Figure 2.1: Pseudo-CAPPI 1500m for the radar of Wideumont derived from 5 scans at different elevation angles (in degrees).

Large hail stones give rise to very high reflectivities that could not be obtained from rain drops. Mason (1971) proposes a reflectivity threshold of 55 dBZ for distinguishing between rain and hail. This method is successful in case of severe hailstorms but does not allow to distinguish between heavy rain precipitation and relatively light hail precipitation.

A slightly different method makes use of the **Maximum-reflectivity** product (MAX) instead of the Pseudo CAPPI. The MAX product gives the highest measured reflectivity value for each vertical column. This product allows detecting high reflectivity values present at higher levels than the Pseudo-CAPPI level. In principle, a threshold criterion based on this product allows detecting hail in developing thunderstorms cells before hail precipitation reaches the ground.

Some methods make use of radar observations together with other sources of information. **Auer** (1994**)** proposes a method which combines radar reflectivity data with infrared cloud-top temperature from satellite imagery. This method has been extensively tested on hail cases in New Zealand and performs much better than the CAPPI method. The cloud top temperature provides additional information on the vertical extension of the thunderstorm cells.

In the United States, the so-called Weather Surveillance Radar-1988 Doppler (WSR-88D) system is the operational radar network system producing meteorological and hydrological analysis products (Crum and Alberty, 1993). The original hail detection algorithm used in the WSR-88D system is based on the presence of seven hail indicators (Smart and Alberty, 1985). After testing is completed, a storm is given one the following four hail labels (positive, probable, negative or unknown).

An enhanced hail detection algorithm has been developed at the National Severe Storms Laboratory (NSSL, USA) and replaces now the original algorithm (Kessinger et al., 1995; Witt et al., 1998). The new algorithm estimates the probability of hail (any size), probability of severe-size hail (diameter ≥ 19 mm), and maximum expected hail size for each detected storm cell. The detection of hail of any size is based on the criterion proposed by **Waldvogel et al. (1979).** The probability of hail is derived from the difference between the maximum height at which a reflectivity of 45 dBZ is observed (H_{Z45}) and the height of the freezing level (H_{T0}) (Fig. 2.2). When the height difference is larger than 1.4 km, a positive indication of hail exists. The probability of hail increases with the height difference (Fig. 2.3). A 100 % probability is obtained for a height difference of 6 km.

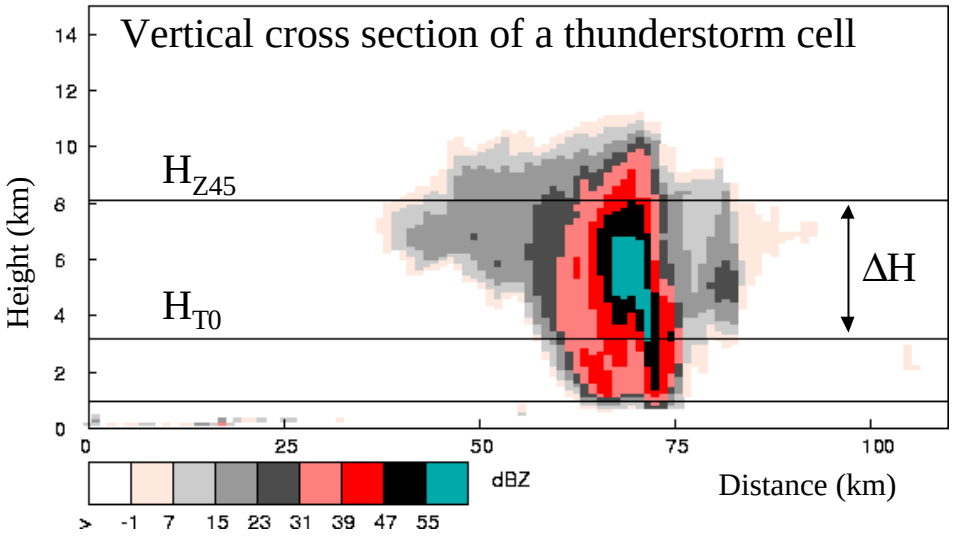

Figure 2.2: Criterion of hail detection proposed by Waldvogel et al. (1979). From Iwan Holleman (KNMI).

The performances of the new algorithm have been evaluated through comparison with ground-truth data collected during a field experiment in the summer months of 1992 and 1993. Kessinger et al. (1995) note a significant improvement with respect to the initial version. The hail detection method based on Waldvogel has been operationally implemented at KNMI (Royal Netherlands Meteorological Institute) and tested on an extended verification dataset in the summer months of 1999 and 2000 (Holleman, 2001). The results show that this method performs substantially better than any other tested methods. The verification results have been used to adjust the function which relates the probability of hail (POH) to the height difference between the freezing level and the maximum height of the 45 dBZ reflectivity.

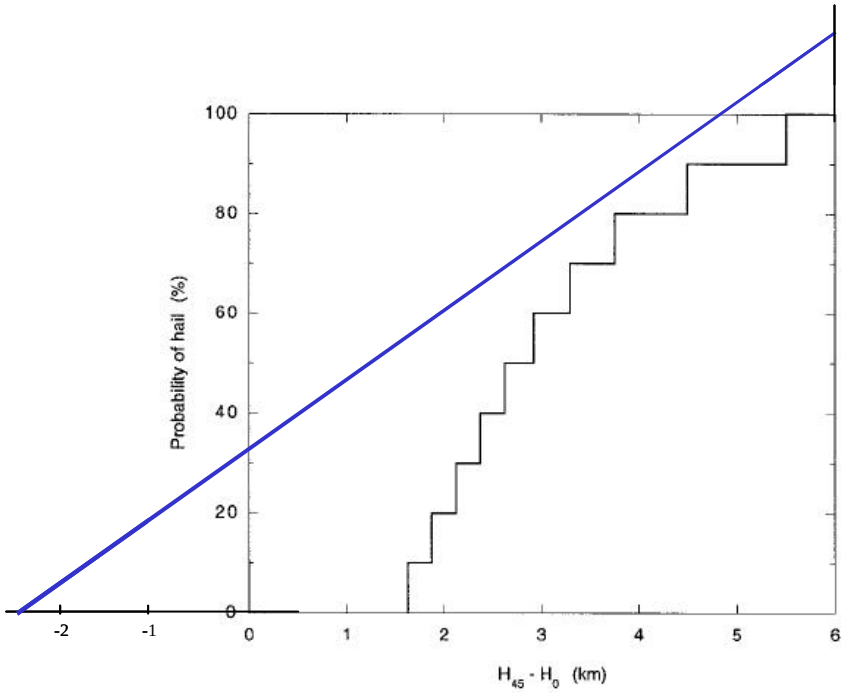

Figure 2.3: Probability of hail as a function of the difference between the maximum height at which a reflectivity of 45 dBZ is observed (H_{Z45}) and the height of the freezing level (H_{T0}). The black line gives the relation used by Witt et al. (1998) and the blue line the expression obtained by Holleman (2001) (figure adapted from Witt et al. (1998)).

The following expression is currently used in the operational hail detection algorithm at KNMI:

$$POH = 0.319 + 0.133\,\Delta H\,(km), \quad \Delta H = H_{Z45} - H_{ZT0} \qquad (1)$$

As can be seen on Fig. 2.3, the linear expression obtained by Holleman (2001) differs significantly from the original relation used by Witt et al. (1998). This is probably due to differences in climatological conditions associated with hail. In particular, the climatology of the height of the freezing level may significantly influence the POH relation.

As mentioned above, the NSSL has also developed algorithms for the detection of severe hail (diameter ≥ 19 mm), and the prediction of maximum expected hail size (Witt et al., 1998). The severe hail algorithm is based on a severe hail index (SHI) derived from the vertical profiles of reflectivity and temperature. The vertical profile of reflectivity is first converted in a vertical profile of hail kinetic energy flux and then vertically integrated using a temperature-based weighting function. The maximum expected hail size is also derived from the SHI using a simple empirical relationship. It must be noted that the verification of severe hail detection algorithm and even more of maximum size prediction is extremely difficult given the highly sporadic nature of severe hail reports.

The vertically integrated liquid water (**VIL**) is another indicator of the severity of a storm cell which was introduced by Greene and Clark (1972). Reflectivity values can be converted to liquid water contents using a semi-empirical relationship similar to the Z-R

relationship used for the conversion of reflectivities to precipitation rates. The vertical integration of the liquid water content is the VIL. Discrimating between thunderstorms with and without hail using VIL only is however not straightforward since there is a large variability in the VIL threshold associated with the presence of hail. A normalized VIL has been proposed by Amburn and Wolf (1997) : the VIL is divided by the height of the top of the thunderstorm cell. This top can be for example determined as the maximum height with a 7 dBZ reflectivity value. The threshold for the **normalized VIL** is supposed to be more universal than the VIL threshold. Nevertheless there is still no agreement on the most appropriate threshold for operational hail detection method using a normalized VIL indicator.

2.3 Discussion

In the previous section, we have presented various methods which have been proposed for detecting hail using single-polarization radars. In the framework of this study, we have tested one of these methods on a number of hail cases observed in Belgium in the summer 2002. The selected method must be performant and reliable but simple enough for allowing a future operational implementation at the weather office.

It is beyond the scope of the present study to perform an intercomparison of various methods and to evaluate their performances on the collected hail dataset. Such study has been recently carried out at KNMI by Holleman (2001). Eight different methods have been compared and verified using a large number of hail reports collected in The Netherlands. The evaluation of the different methods is based on a number of verification scores: the probability of detection, the false alarm ratio and the critical success index. The results show that the method of Waldvogel based on the height difference (ΔH) between the freezing level and the echotop 45 dBZ scores best. After having tested this method in semi-operational conditions, the relationship between ΔH and the probability of hail has been adjusted to best fit the on-ground observational data. The method of Waldvogel has also the advantage of a relatively simple implementation. It is mainly based on radar reflectivity data. The only external parameter that is needed is the height of the freezing level, which can be estimated from radiosonde data or from a regional numerical weather prediction model. At KNMI, the freezing level is extracted from the HIRLAM model short-term weather forecast. Some methods require more external data like vertical profiles of temperature (Sever Hail Index method, Witt et al. (1998)) or cloud top temperature from infrared satellite data (method of Auer (1994)), which may complicate their operational implementation and routine use.

Significant regional differences in the performances of a given hail detection algorithm can be expected. In the USA, the method of Waldvogel has been extensively tested using special field project data in the state of Colorado. As mentioned by Witt et al. (1998), it is “possible, and perhaps even likely” that the performances of the algorithm will be poorer in other regions of the United States. These differences are related to the different natures of storms generating hail. The intercomparison study performed at KNMI is of great interest for meteorologists in Belgium since the climatological conditions in Belgium and The Netherlands are similar and it is likely that the thunderstorms responsible for hail are of the same type. For these reasons, we have chosen to select the Waldvogel method using the POH relationship obtained by Holleman for implementation and testing against hails cases observed in Belgium.

3 Hail cases during summer 2002

3.1 Hail reports

The RMI climatological network comprises about 250 stations. In most stations, measurements are manually collected by an observer. During spring 2002, about 50 observers considered as the most reliable were asked to be particularly attentive to hail and in case of hail event to make a short report containing the exact time of the observation and the size of the observed hailstones. At the end of the summer, 32 reports had been collected. Some reports were also spontaneously sent by weather amateurs.

Time (LT)	Place	Size (cm)	Distance (km)	H_{T0} (km)	Code
April 19					
15h30 – 16h	Corbais	~ 0.5		1.3	A1
May 26					
12h20 – 12h30	Mouscron	~ 0.5	186	1.7	B1
12h54 – 13h01	Vinkt	~ 0.5	189	1.7	B2
13h10 – 13h13	Zomergem	~ 0.5	191	1.7	B3
15h17 – 15h35	Quevy-le-Petit	~ 0.5	123	1.7	B4
16h35 – 16h37	Sint-Pieters-Rode	~ 0.5	121	1.7	B5
16h37 – 16h42	Korbeek-Lo	~ 0.5	119	1.7	B6
16h50	Morkhoven	~ 0.5	143	1.7	B7
June 4					
20h45 – 20h55	Lessines	~ 2	149	3.1	C1
20h00 – 21h20	Geraardsbergen	~ 0.5	153	3.1	C1
June 14					
22h15 – 22h30	Néchin	~ 0.5	180	3.6	D1
22h21 – 22h25	Mouscron	~ 1	186	3.6	D1
22h30 – 22h35	Herinnes	~ 2	176	3.6	D1
22h42 – 22h45	Izier	~ 2	53	3.6	D2
23h00 – 23h05	Zele	~ 0.5	164	3.6	D3
23h58 – 24h00	Sint-Pieters-Rode	~ 1	121	3.6	D4
July 30					
16h20 – 16h30	Daussoulx	~ 0.5	81	3.8	E1
16h45 – 16h57	Waasmont	~ 0.5	96	3.8	E2
17h05 – 17h28	Godarville	~ 0.5	108	3.8	E3
17h14 – 17h35	Court-St-Etienne	~ 0.5	104	3.8	E4
19h20 – 19h25	Izier	~ 0.5	53	3.8	E5
Aug 3					
14h49 – 16h15	Vinkt	~ 0.5	189	2.5	F1
17h00 – 17h30	Kinrooi/Kessenick	~ 1	138	2.5	F2

Table 1: Inventory of the selected hail cases in the summer 2002. The size is the diameter of the observed hailstones, the distance is the distance from the weather radar of Wideumont, H_{T0} is the height of the freezing level.

Hail reports without precise indication of time and place were rejected as well as reports with very small hailstones (diameter clearly smaller than 0.5 cm). Some of the observed hail cases had also to be rejected since radar data were missing at the time of observation. As a result 23 observed hail cases were selected. Most of these cases correspond to hailstones of relatively small size (diameter around 0.5 cm). Three reports indicate hail stone with a diameter around 1 cm and three reports mention hailstones around 2 cm. Table 1 presents the inventory of the selected hail cases.

3.2 Meteorological analysis

April 19, 2002

A quasi stationary Upper Level Low (ULL) covers our areas from southeast England to west Germany (see Fig. 3.1). At low levels the pressure field is rather high but quasi uniform and no frontal zones have been analysed in our areas. At mesoscales a few convergence lines are detected. The largest one reaches about 100 kilometres. The radiosounding performed at Uccle indicates a high convective instability in the atmosphere. The vertical wind shear is weak, at least in the lower layers up to 700 hPa. The isotherm of zero degree is situated around 1300 m and the tropopause level reaches only 7000 m. So the thickness of the below zero cumulonimbus approximates 6000 m.

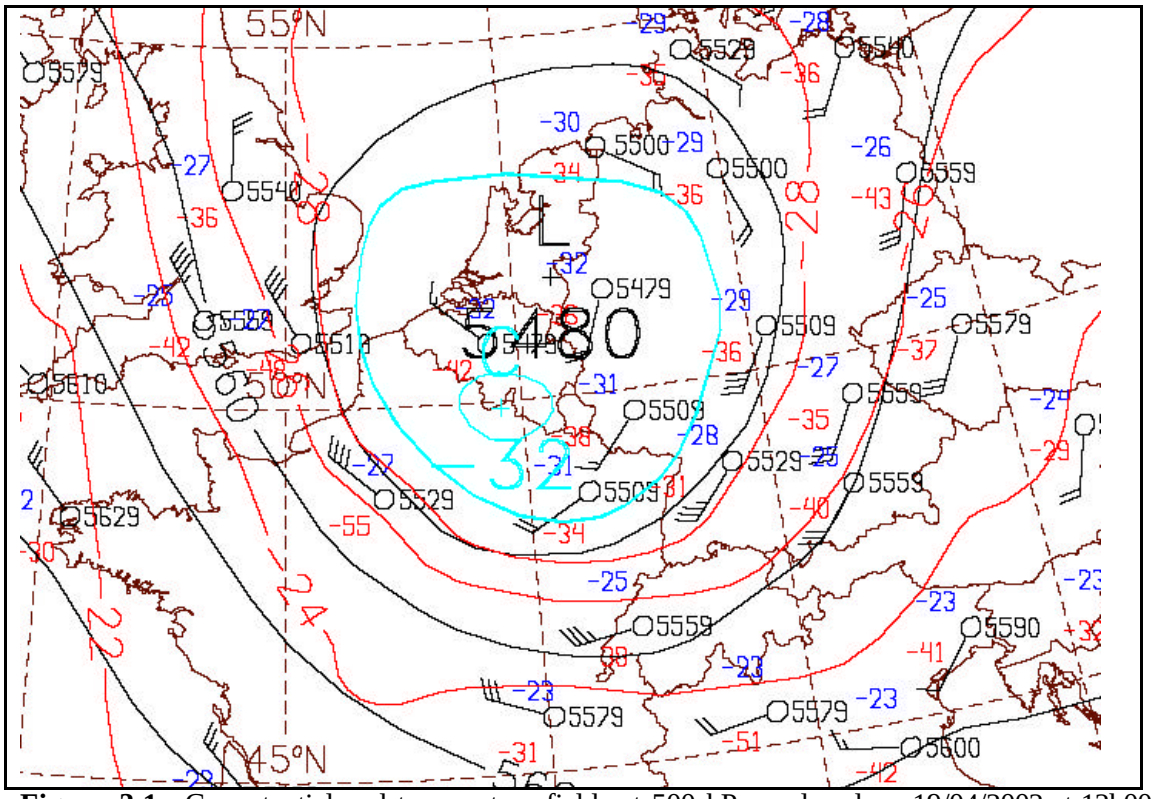

Figure 3.1 : Geopotential and temperature fields at 500 hPa analysed on 19/04/2002 at 12h00 U.T.C. are represented by black and coloured isolines respectively. The quasi concentric isolines patterns are quite typical for an Upper Level Low.

May 26, 2002

A fast southwesterly perturbed flow is associated with a depression centered over the British Islands. Shower lines at mesoscales are mostly observed when the main trough is crossing our areas around noon and in the cold air behind it (between 12h00 and 18h00 U.T.C.). A maximum of cyclonic vorticity and cold air advection is detected on the polar side of a jet streak which extends from the center of France to Belgium around 12h00 U.T.C. (Fig. 3.2). The radiosoundings in our areas indicate both a high convective instability and a strong vertical wind shear. The isotherm of zero degree is situated around 1700 m and the tropopause level reaches about 10 km.

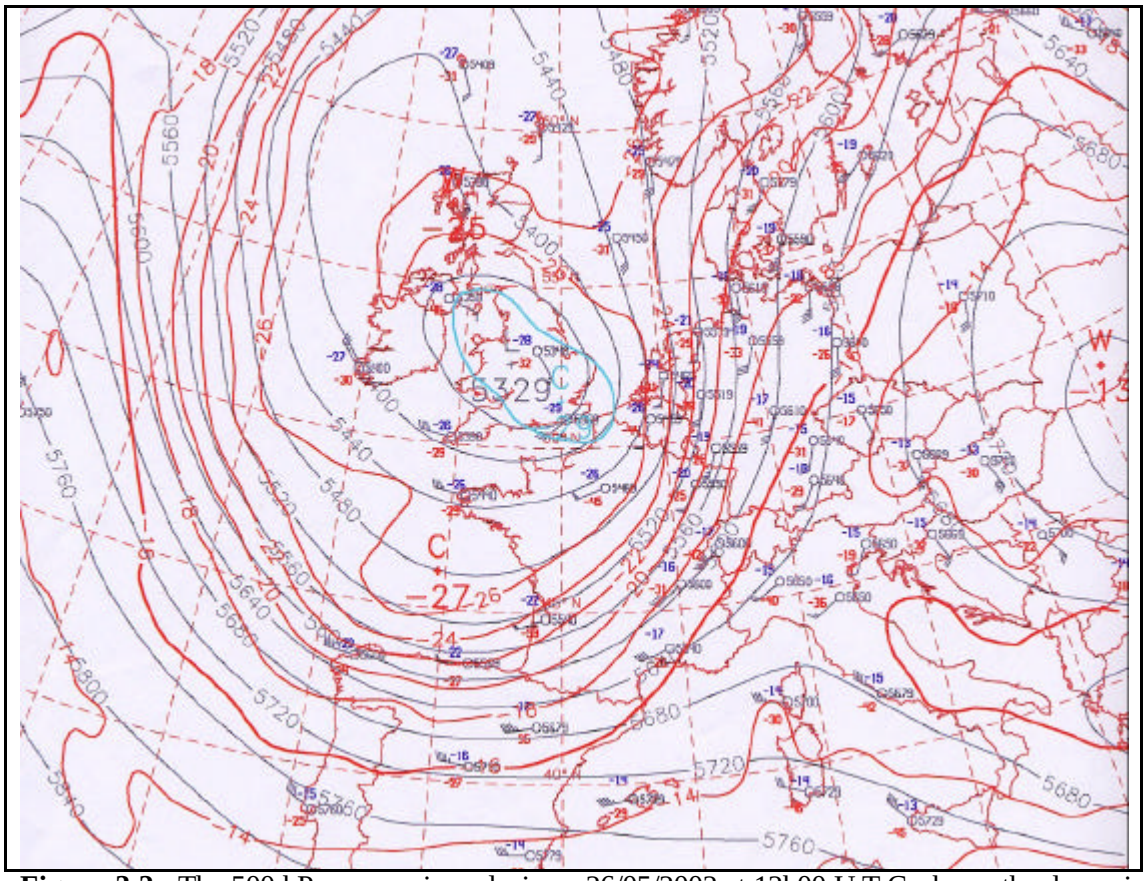

Figure 3.2 : The 500 hPa upper-air analysis on 26/05/2002 at 12h00 U.T.C. shows the dynamic trough crossing the northern part of France and our areas.

June 4, 2002

A complex low pressure area deepens on western Europe mainly from France to West Germany. The deepening low induces a southerly advection of warm and humid air characterized by high wet bulb potential temperatures in the lower layers. In the afternoon a mesoscale surface high develops on the North Sea and contributes to the formation of a sharp convergence line which separates the cold and dry air from the above mentioned warm and humid air. At 18h00 U.T.C. this convergence line extends from the north of France to the southwest of Belgium (Hainaut) and the south of Netherlands (Fig. 3.3). The radiosoundings in our regions confirm the presence of warm and humid air in the lower layers surmounted by drier and more stable air in the middle layers of the troposphere. The vertical wind shear is moderate. In the warm air the isotherm of zero degrees lies around 3100 m and the tropopause is situated at 11 km.

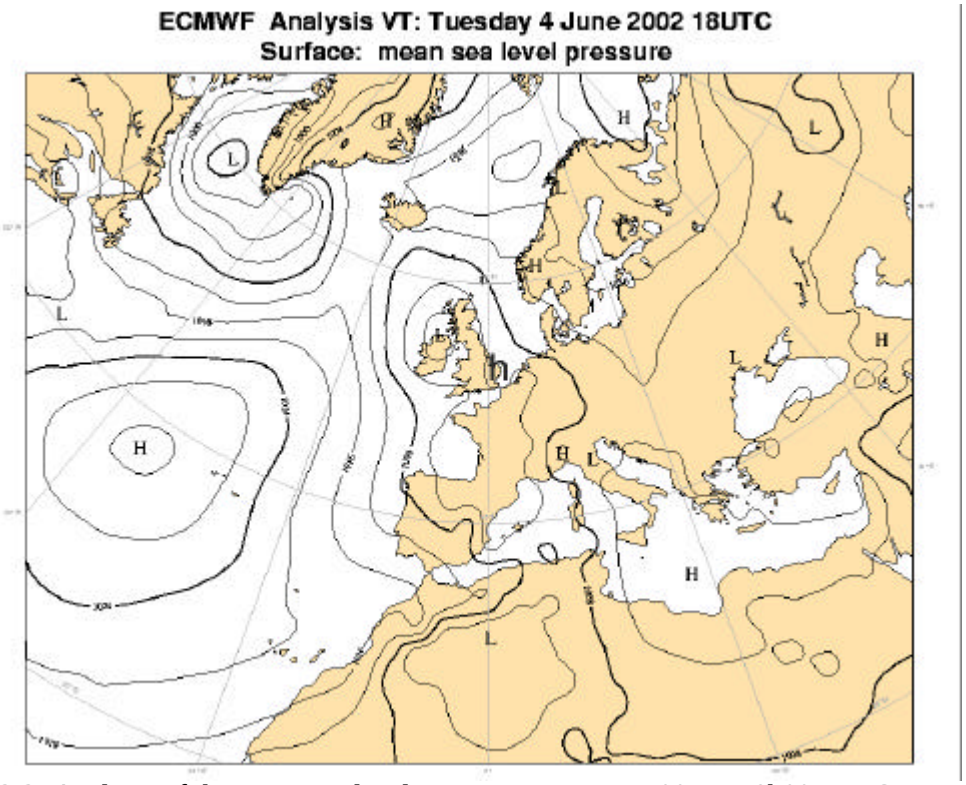

Figure 3.3 :Analysis of the mean sea level pressure on June 4 2002 at 18h00 U.T.C. : a complex low pressure covers the major part of western Europe from the British Islands to France and Spain. At mesoscales a high pressure area (h) is situated over the North Sea and a trough delineates the convergence line over Belgium

June 14, 2002

A thermal trough progresses from western France to our areas in the afternoon and the evening. Warm and humid air is advected in the lower layers of the troposphere. Figure 3.4 indicates the progression of the thermal trough over the northwestern part of France and our areas. This thermal trough is coupled to a more dynamic upper-air wave moving northeasterly over England and the Channel.

Several convergence lines are developing in the thermal trough. One of them is crossing the western part of Belgium in the evening. The radiosoundings in our areas indicate a high convective instability in the lower levels mostly in the evening and a strong vertical wind shear. The isotherm of zero degree lies around 3600 m and the tropopause around 12 km.

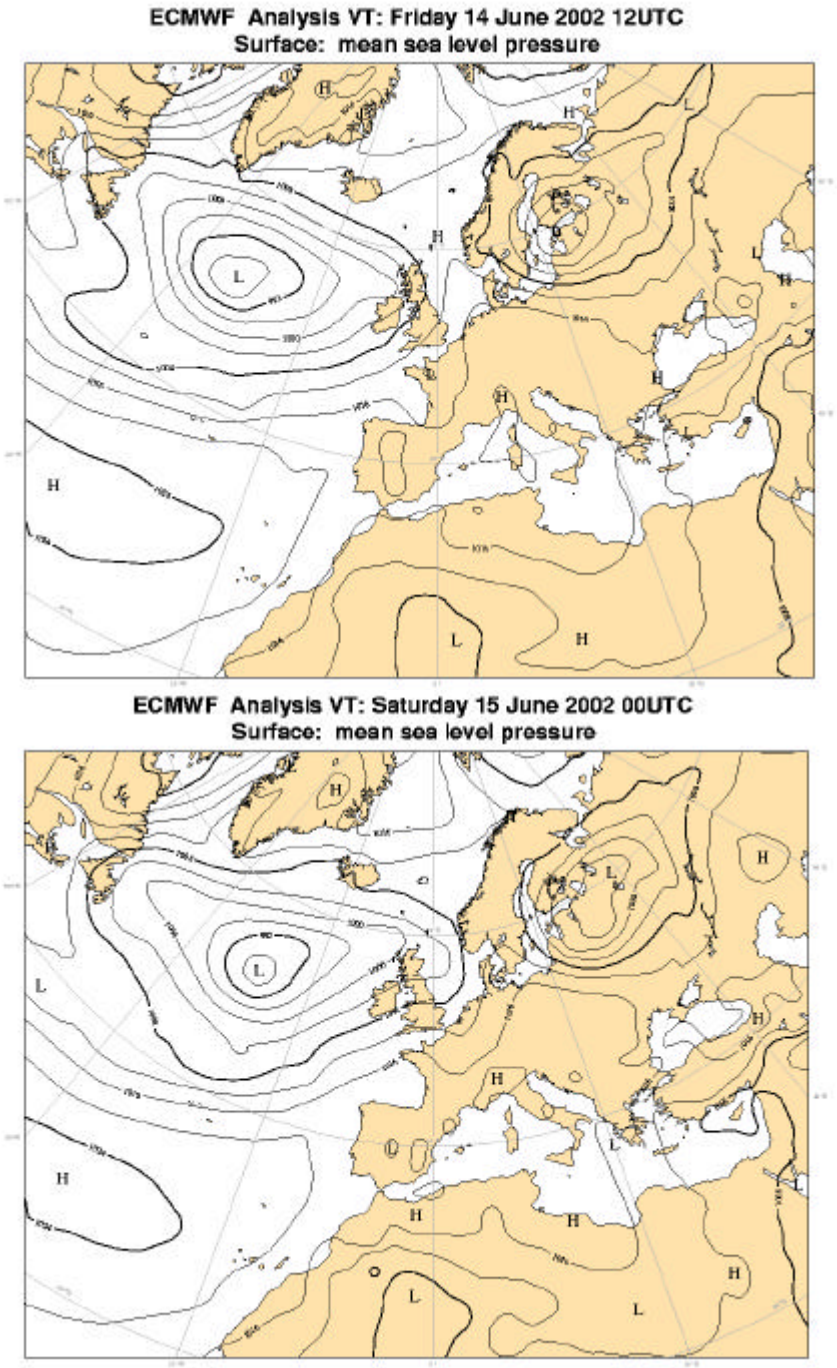

Figure 3.4 : Analysis of the mean sea level pressure field, respectively on June 14 2002 at 12h00 U.T.C. and June 15 2002 at 00h00 U.T.C. A rather flat thermal trough is analysed over the western part of France and moves to our regions.

July 30, 2002

A large thermal trough extends from the centre of Europe and the Alps to our areas and the southeastern part of England. Warm and humid air in the lower layers of the tropopause covers a rather flat trough in the surface pressure field (Fig. 3.5).This situation is largely decoupled from the upper air waves over the British Islands. Several convergence lines are developing at mesoscales over our areas mostly during the afternoon. The radiosoundings in our areas indicate a rather homogeneous convective

unstable air mass with a weak vertical wind shear. The level of the isotherm of zero degree lies around 3800 m and the tropopause around 12000 m. In this environment the below zero cumulonimbus thickness reaches about 9000 m.

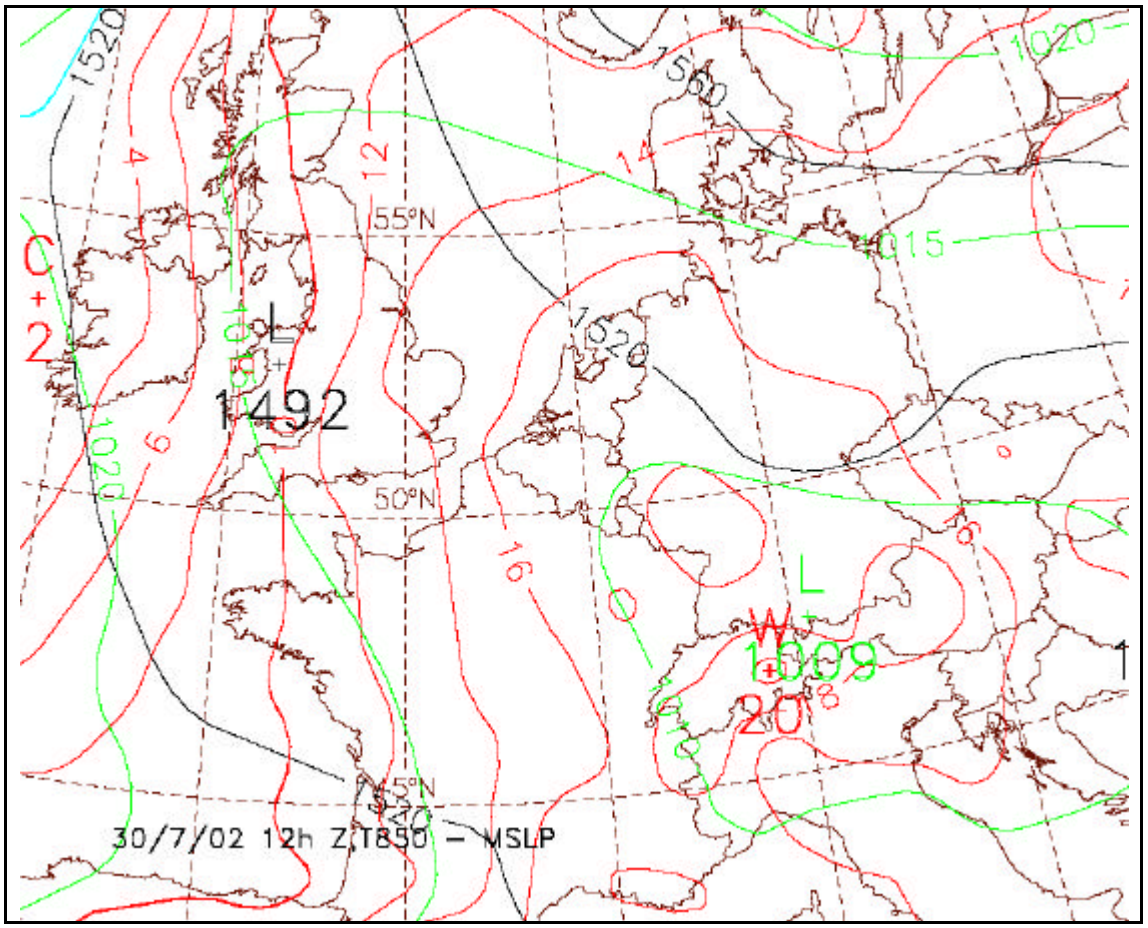

Figure 3.5 : The mean sea level pressure, 850 hPa geopotential, and 850 hPa temperature fields are represented on 30/07/2002 at 12h00 U.T.C by green, black and red isolines, respectively. The warm (and humid) air tongue covers the surface trough area in the lower layers of the troposphere. This situation is a typical signature of a thermal trough.

August 3, 2002

This situation is rather similar to the hail case of the 19th of April 2002. An Upper Level Low moves very slowly northeasterly over the northern part of France and our areas (Fig. 3.6). At the surface the pressure field is rather flat and from noon on convergence lines are developing at mesoscales over our regions. In the evening one of these convergence lines extends more widely over northern France to the western part of Belgium. The radiosoundings confirm the presence of deep unstable air with a slightly more pronounced vertical wind shear in the upper part of the troposphere. The isotherm of zero degree lies at 2500 m and the tropopause around 10 km.

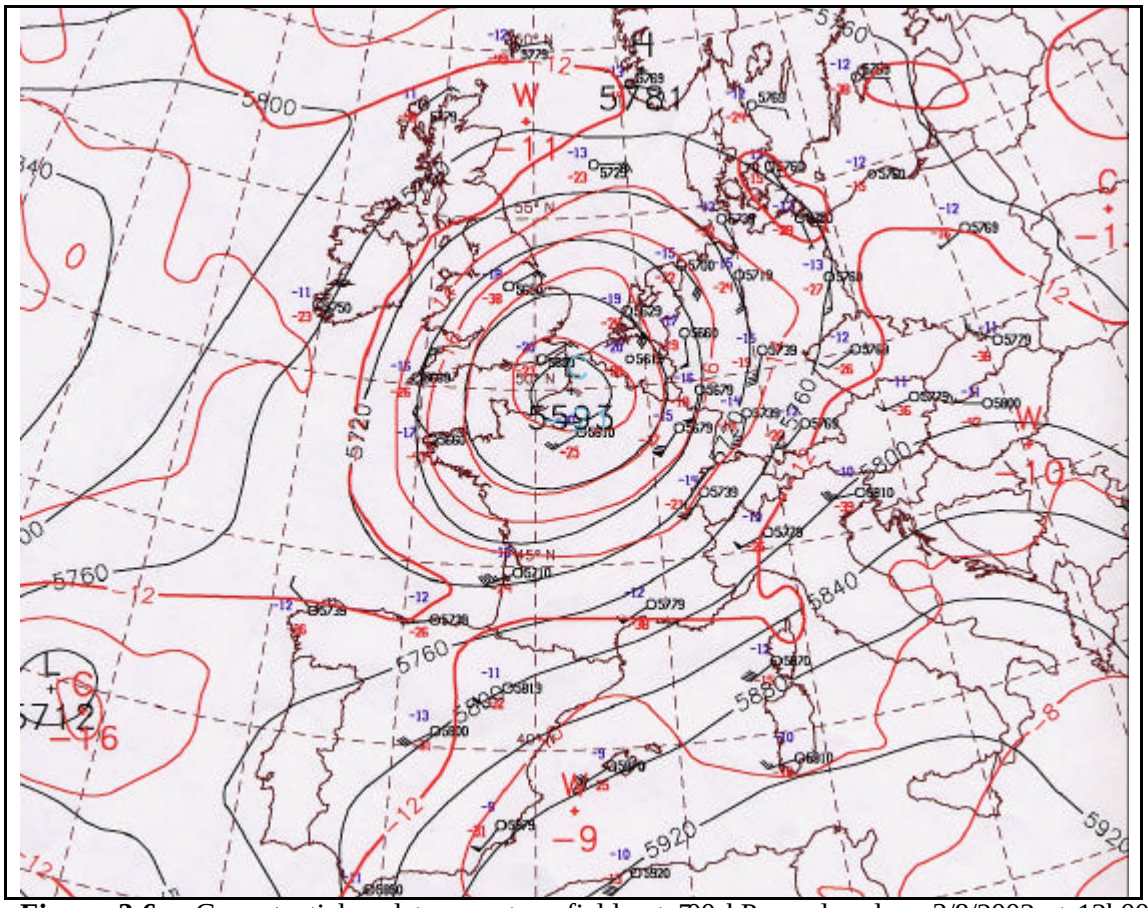

Figure 3.6 : Geopotential and temperature fields at 500 hPa analysed on 3/8/2002 at 12h00 U.T.C. are represented by black and red isolines respectively. As for the 19th of April 2002 these upper-air fields indicate a clear cyclonic circulation associated with a cold air depression centred over the northern part of France and our areas.

4 Results of radar-based hail detection

4.1 Algorithm implementation

Radar data are provided by the radar of Wideumont operated by the Royal Meteorological Institute of Belgium. The radar performs every 15 minutes a volumic scan at 10 different elevation angles between 0.5 and 17.5 degrees. The paths of the different beams in standard atmospheric conditions are depicted in Fig. 4.1. Only the centres of the radar beams are drawn. It must be kept in mind that the beamwidth is 1 degree in both horizontal and vertical directions. At a distance of about 100 km, the lowest radar beam intercepts a 2 km-depth atmospheric layer.

Data are collected at an azimuthal increment of 1 degree and a range increment of 500 m. The maximum range is 240 km. From these volumic data, the echotop-45 dBZ is determined for each azimuth and range as the height of the highest radar beam where a reflectivity at least equal to 45 dBZ is measured. For each of the selected hail cases, the height of the freezing level is determined from radiosonde data and NWP model analysis. It must be noted that the height of the freezing level (H_{T0}) does not need to be very accurately estimated since the sensitivity of the probability of hail as calculated by expression (1) with respect to this parameter is not very high. A 1 km difference in H_{T0} corresponds to a difference in POH of 13 %.

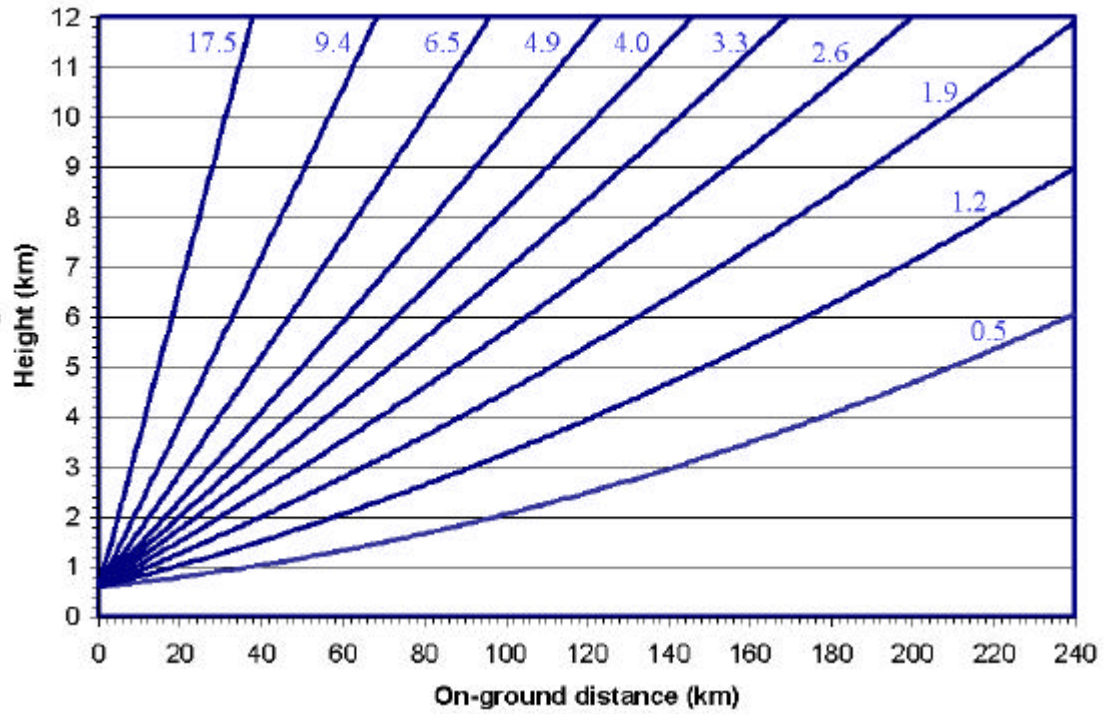

Figure 4.1 : Paths of the radar beams for the 10 elevations of the volumic scan performed by the radar of Wideumont.

4.2 Results for the observed hail cases

The hail detection algorithm was applied to the 23 selected hail cases. Radar volumic files from which the echotop-45 dBZ is calculated are available every 15 minutes. For each case, the observed period of hail is given in Table 1. However, a larger time window has been considered for the calculation of the probability of hail. The time window must be extended with respect to the observed time period for different reasons.

A1 Corbais 19/04 d=100 km

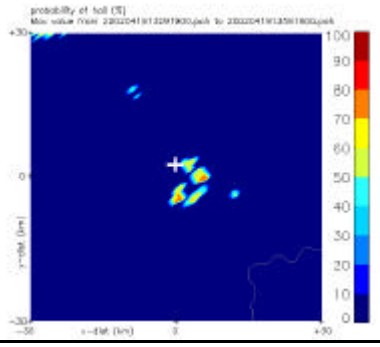

B1 Mouscron 26/05 d = 186 km

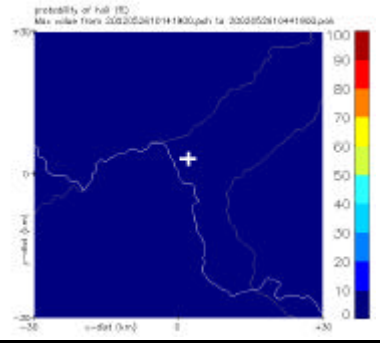

B2 Vinkt 26/05 d = 189 km

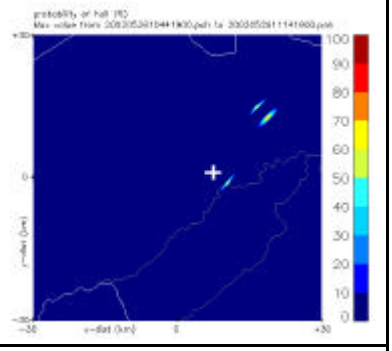

B3 Zomergem 26/05 d = 191 km

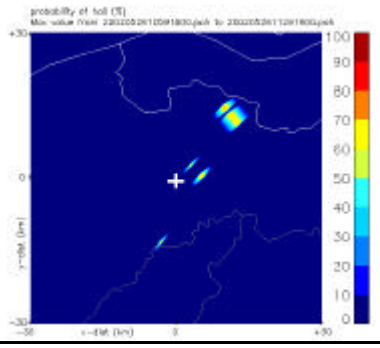

B4 Quevy 26/05 d = 123 km

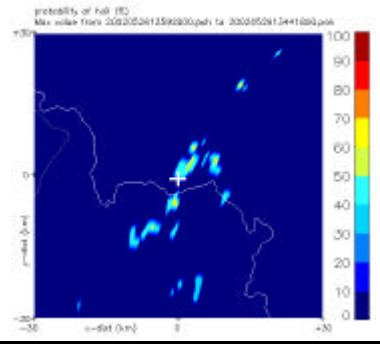

B5 Sint-Piet.-R. 26/05 d = 121 km

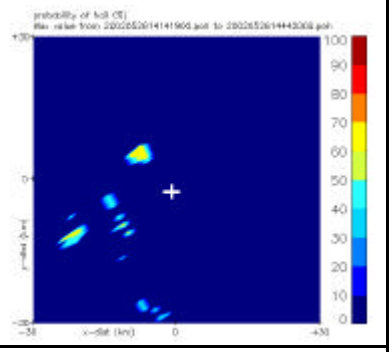

B6 Korb.-Lo 26/05 d = 119 km

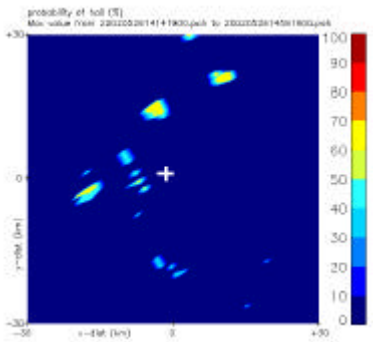

B7 Morkhov. 26/05 d = 143 km

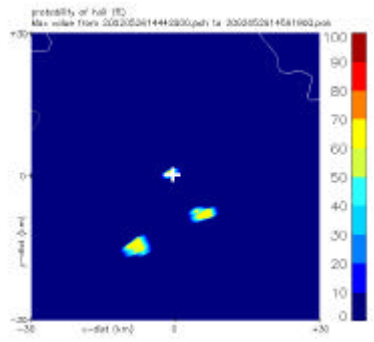

C1 Lessines 4/6 d = 149 km

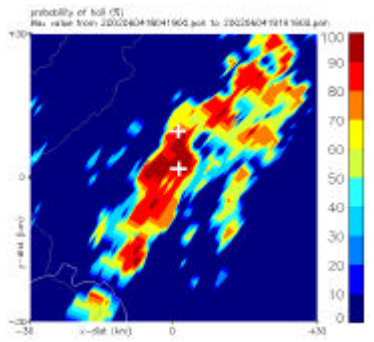

D1 Néch./Mousc. 14/6 d = 180 km

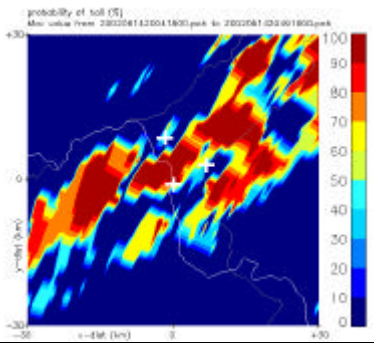

D2 Izier 14/6 d = 53 km

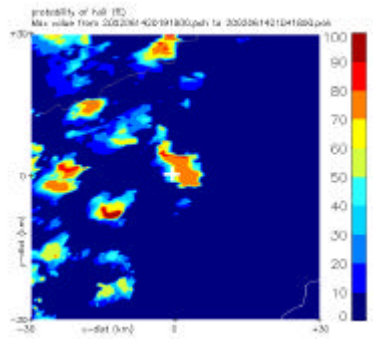

D3 Zele 14/6 d=164 km

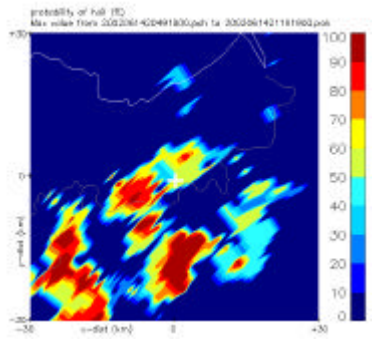

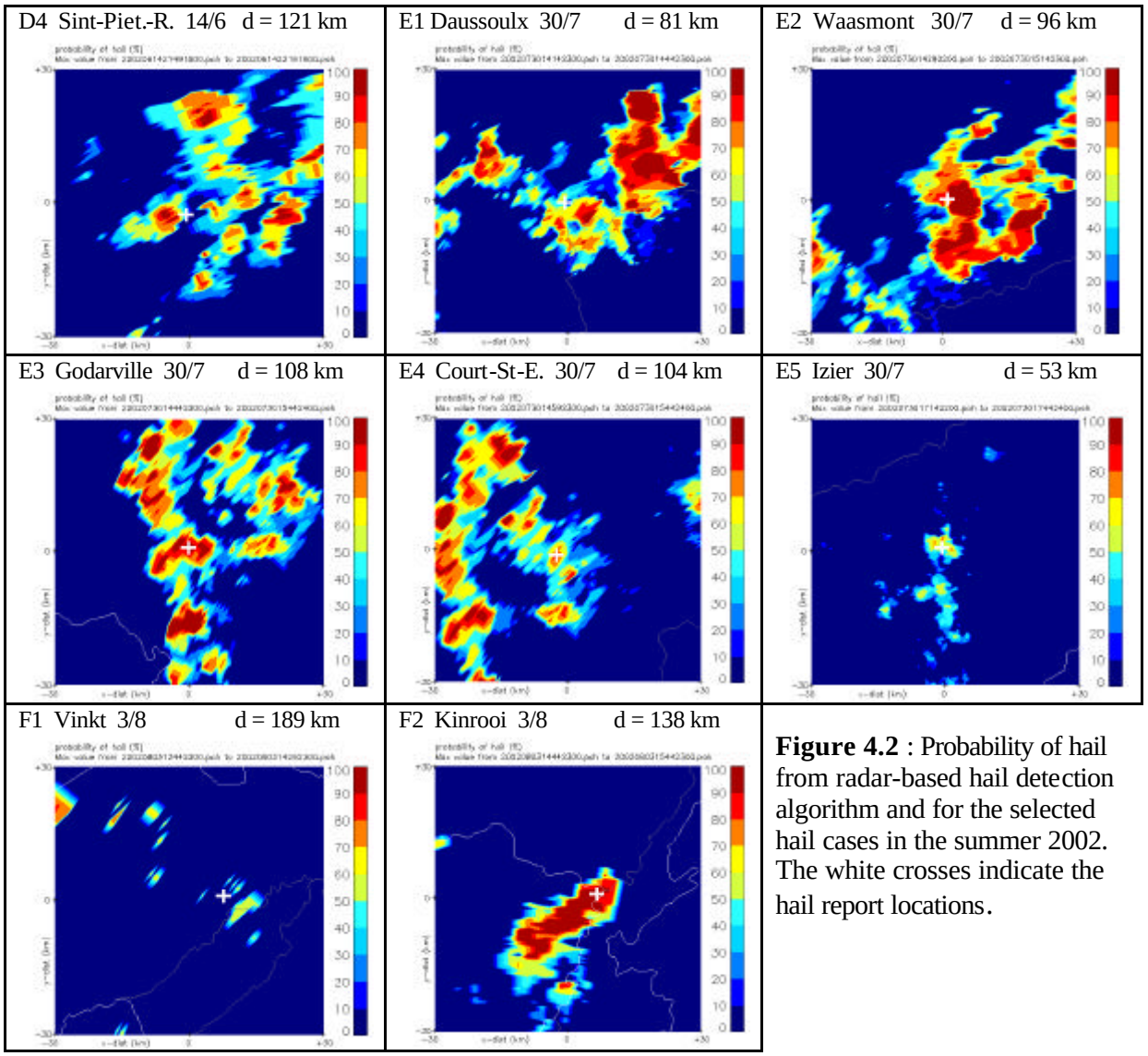

Figure 4.2 : Probability of hail from radar-based hail detection algorithm and for the selected hail cases in the summer 2002. The white crosses indicate the hail report locations.

First some uncertainties in the reported time of observations must be taken into account. Secondly, the time resolution of the radar volumic data is 15 minutes. And third, a delay between the presence of a hail core at a given altitude and hail precipitation at the ground level must be considered. We have chosen to add a 15 minutes buffer zone on both ends of the observed time period of hail.

All the radar data files within the extended time window are analysed to calculate for each pixel the probability of hail. For each hail case, the probability of hail is then determined as the maximum value obtained within the time window. The results obtained for the 23 hail cases are shown in Fig. 4.2. The probability of hail is given as a percentage between 0 and 100 %. The visualization domain is a 60 x 60 km2 square approximately centred on the location of the hail report. The white cross indicates the exact location. Some hail cases are presented in a single plot and a single time window since the reports are very close to each other in time and space. The two cases on June 4 (code C1 in Table 1) have been gathered in a single plot and three cases on June 14 as well (code D1). The code, location, date and distance to the radar are indicated above each plot.

The results show that in most cases a significant probability of hail is obtained near the location of hail report. There is only one case where no hail is detected on the selected time window and on the 60x60 km^2 domain (B1: Mouscron, May 26)). All the reported hail cases on May 26 give relatively low POH. This is probably due to the fact that hail was quite moderate and that most of the locations are at long distance from the radar. At long distance, even the lowest radar beam may overshoot the high reflectivity core of the thunderstorm cell associated with hail. If no reflectivity higher than 45 dBZ is measured, a zero POH is given by the hail detection algorithm.

For 22 cases on 23, a probability of hail at least equal to 50 % is found at a smaller distance than 10 km from the hail report location. For 16 cases on 23, a POH at least equal to 70 % is found. Errors on the localization of the hail events are partly due to the "jumping effect" caused by the displacement of the thunderstorm cells within the 15 minute time interval between successive radar snapshots (Fig. 4.3). For a storm moving at a 10 m/s speed this displacement reaches 9 km. Spatial shift between the reflectivity core at high altitude (which determines the echotop 45 dBZ) and the on-ground location of hail also introduces errors on the localization of hail events. Assuming a typical hail fall speed of 10 m/s (Böhm, 1989), a hailstone at a 6-km height will take 10 minutes for reaching the ground. Even with a moderate horizontal wind drift, the horizontal displacement of the hailstone can reach a few kilometres.

As far as the spatial structure of hail thunderstorms is concerned, comparisons between reflectivity data collected by the radars of Wideumont and The Bilt (The Netherlands) were recently made in collaboration with KNMI. The comparisons concerned thunderstorms located between the two radars and the results show that the spatial structure of the hail thunderstorms as seen by the two radars was very similar (Delobbe and Holleman, 2003).

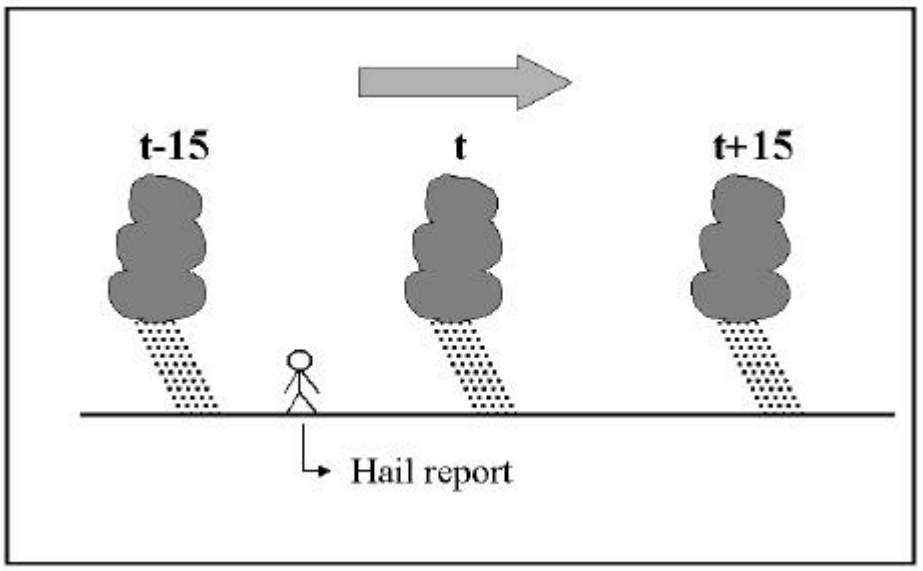

Figure 4.3: Illustration of the "jumping cells" effect due to the 15-min time interval between radar volumic data files.

4.3 Evaluation and discussion

When a hail detection algorithm is operationally used for providing hail warnings, a threshold must be applied to the probability of hail (POH). A hail warning will only be given if the probability of hail exceeds the selected threshold. The performance of the hail warning will depend on the threshold. A low threshold will ensure a high probability of detection but will also increase the probability of false alarm.

As mentioned above, errors in the localization of hail falls are unavoidable due mainly to the limited time resolution of the radar observations. Therefore a localization tolerance must be introduced for the evaluation of the performance of a hail detection algorithm.

Table 2 shows the performance of the tested algorithm for the 23 selected hail cases. The detection rate, i.e. the number of detected cases on the number of observed cases, is given as a function of the POH threshold and the localization tolerance. For example, when a 70 % POH threshold is used and a 10 km tolerance on the localization, 16 cases on 23 are detected by the algorithm.

	30 %	**50 %**	**70 %**	**90 %**
5 km	20/23	20/23	16/23	10/23
10 km	22/23	22/23	16/23	12/23
15 km	22/23	22/23	16/23	12/23
20 km	22/23	22/23	18/23	12/23
30 km	22/23	22/23	18/23	12/23

Table 2: Hail detection rate as a function of the localization tolerance (km) and the probability of hail used as detection threshold (%).

Table 2 shows no difference between the results with a detection threshold of 50 % and 30 %. It means that lowering the threshold from 50 % to 30 % does not increase the number of detected hail cases. With a detection threshold of 50 % and a 5 km localization tolerance, 20 cases on 23 are detected. When the tolerance is set to10 km, 22 cases on 23 are detected, which is a remarkable result. It should be noted that the localization tolerance does not highly influence the detection rate which suggests that the localization errors remain quite limited.

The detection rate decreases with the warning threshold. For a 90 % threshold, about 50 % of the observed hail cases are detected. However, it is worth noting that all the observed cases with hailstones larger than 1 cm are correctly detected with a warning threshold of 90 % and a localization error less than 5 km. A higher probability of hail is associated with larger hailstones.

As mentioned above, a small threshold is needed to maximize the probability of detection of a hail event. However, a low POH threshold will also increase the False Alarm Rate (FAR). The present study based on the collection of a number of hail reports allows to evaluate the ability of the algorithm in detecting hail when hail was actually reported but does not allow to get an idea of the estimated probability of hail when no hail occurred. Our results show that the areas with non zero POH are quite limited, which indicates that the hail detection algorithm is quite restrictive. However,

the present study does not allow a quantitative evaluation of the false alarm rate. The determination of the probability of false alarm is an extremely difficult task due to the sporadic nature of hail. No hail report does not mean that hail did actually not occur. An estimation of the FAR needs an assumption on the fraction of hail events which are not reported. Making such assumption, Holleman (2001) estimates that the FAR using the Waldvogel method may reach 50 %. The method of Waldvogel was also tested at the NSSL (USA) during a field experiment in the Colorado State and a FAR as low as 4% was reported (Kessinger et al., 1995; Witt et al., 1998). Such discrepancies illustrate the difficulty in setting up a robust methodology allowing a correct estimation of FAR.

Without knowledge of FAR, the determination of the detection threshold must be based on the detection rates presented in Table 2. Based upon these results, it seems appropriate to use a warning threshold of 50 % for the detection of hail, and a 90 % threshold for the detection of severe hail events. However, the number of reported hail events remains quite low and a better evaluation of the algorithm performances will be performed in the future when the number of reported hail cases will be larger.

5 Comparison with SAFIR observations

The RMI has been operating a lightning detection system since August 1992. The system is called "SAFIR": Système d'Alerte Foudre par Interférométrie Radioélectrique. It allows the real time detection of lightning activity with a location accuracy of about 1 km and a time resolution of 150 µs. The system is able to distinguish between Intra-Cloud lightning activity (IC) and Cloud-to-Ground lightning activity (CG).

For the various reported hail episodes, the SAFIR data have been compared with the radar data in order to get a first idea of the relation between the electrical activity and the occurrence of hail. The comparison has been made for the 23 selected hail cases. The results obtained for a few representative cases are presented in Fig. 5.1 and 5.2. The same visualisation domain is used for the SAFIR and the radar probability of hail data. The first figure shows the total lightning activity and the radar-based probability of hail for the cases A1 (April 19), B3 (May 26) and C1 (June 4). In the lightning plot, the colours indicate the time within the total displayed period. This allows visualizing the displacement of the electrically active area. The first two cases are representative for a quite low thunderstorm intensity. The lightning activity as well as the probability of hail derived from the radar data are low. For the hail episodes of 19 April and 26 May, the vertical extension of the thunderstorm cells was not very high, the size of the hailstones was around 0.5 cm and the height of the freezing level was less than 2 km (Table 1). These two hail episodes can not be considered as typical hail situations associated with severe thunderstorms but rather as moderately developed convective cells in a relatively cold environment. This is particularly the case for the hail event of 19 April, where the freezing level was as low as 1.3 km. This kind of situation is associated with a relatively low lightning activity compared to severe thunderstorm situations. In contrast, the severe hail episode reported on June 4 is associated with a strong lightning activity and the radar-based probability of hail reaches 100 % in large areas (Fig. 5.1).

The total lightning density, i.e. the number of electrical discharges occurring per square kilometre and per minute is illustrated in Fig. 5.2. The total density identifies the most active areas in the thunderstorm. The comparisons between the radar and SAFIR data are shown for the cases C1 (June 4), D1 (June 14) and E3 (July 30). The comparison shows a very good agreement as far as the spatial structure is concerned. Areas with high POH are associated with high electrical activity. The same feature is found for the other hail cases with high electrical activity.

The localization and timing of the lightning activity and the probability of hail have been further analysed for the severe hail case of Lessines (C1, June 4). Hail was produced by a thunderstorm complex moving north-eastward. The time evolution has been split into 4 time intervals of 30 minutes. For each interval, the probability of hail was calculated using the two radar volumic files collected in the given interval. The comparison between the probability of hail and the cloud-to-ground lightning activity for the 4 time intervals is shown in Fig. 5.3. Again, a very good qualitative agreement between the areas of high POH and the areas of high electrical activity can be observed. The SAFIR system appears as a complementary observational tool with respect to the radar for the real-time detection of severe thunderstorm cells likely to produce hail.

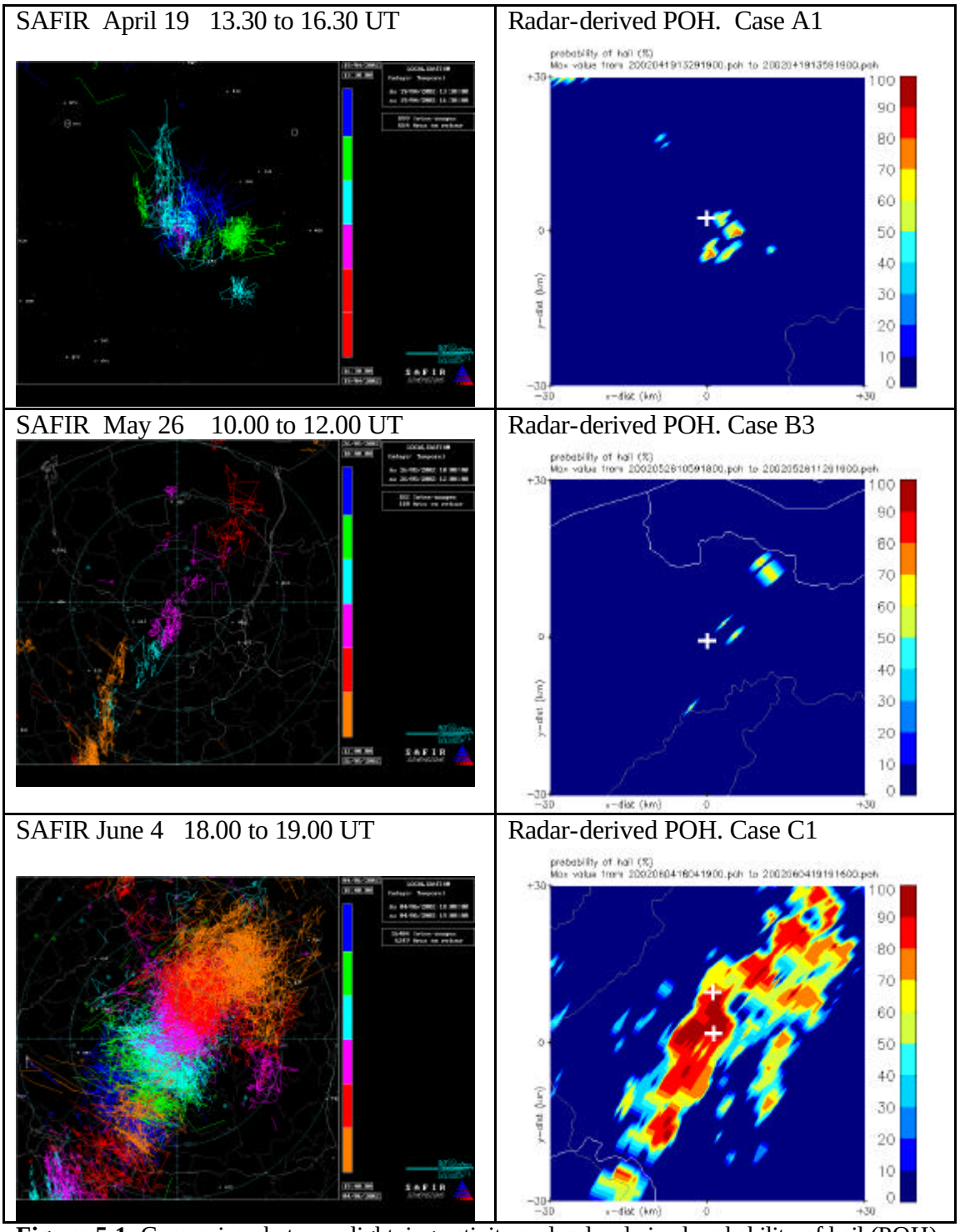

Figure 5.1: Comparison between lightning activity and radar-derived probability of hail (POH) for hail cases A1, B3 and C1.

SAFIR June 4 18.00 to 19.00 UT	Radar-derived POH. Case C1
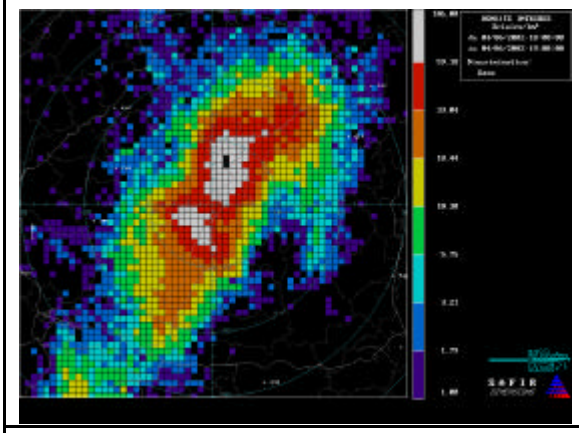	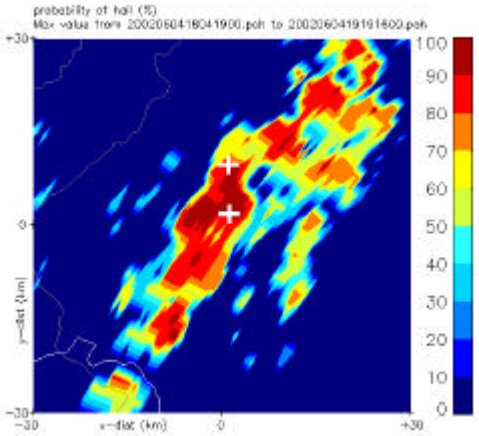
SAFIR June 14 19.00 to 24.00 UT	Radar-derived POH. Case D1
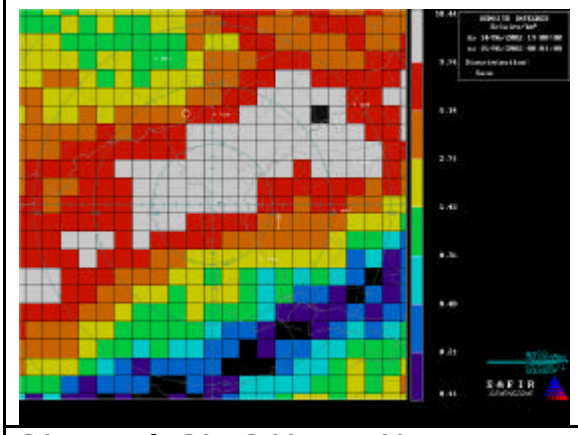	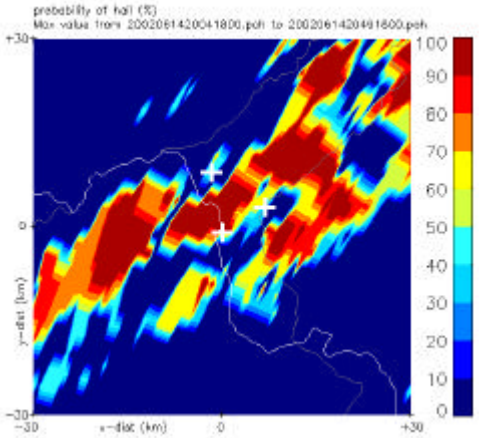
SAFIR July 30 13.00 to 17.00 UT	Radar-derived POH. Case E3
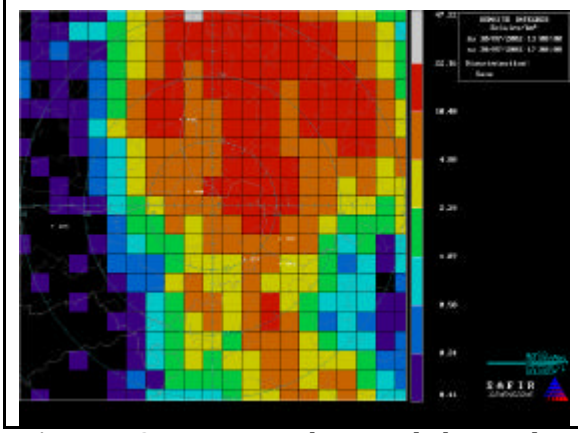	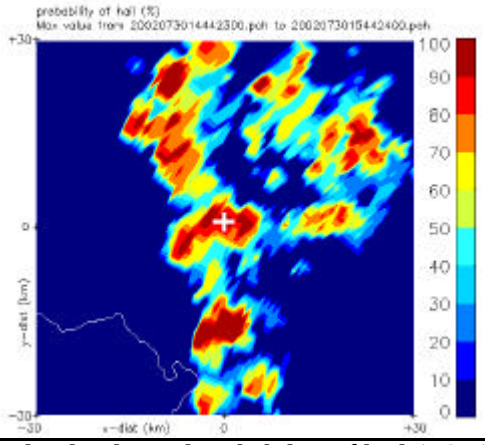

Figure 5.2: comparison between lightning density and radar derived probability of hail (POH) for cases C1, D1 and E3.

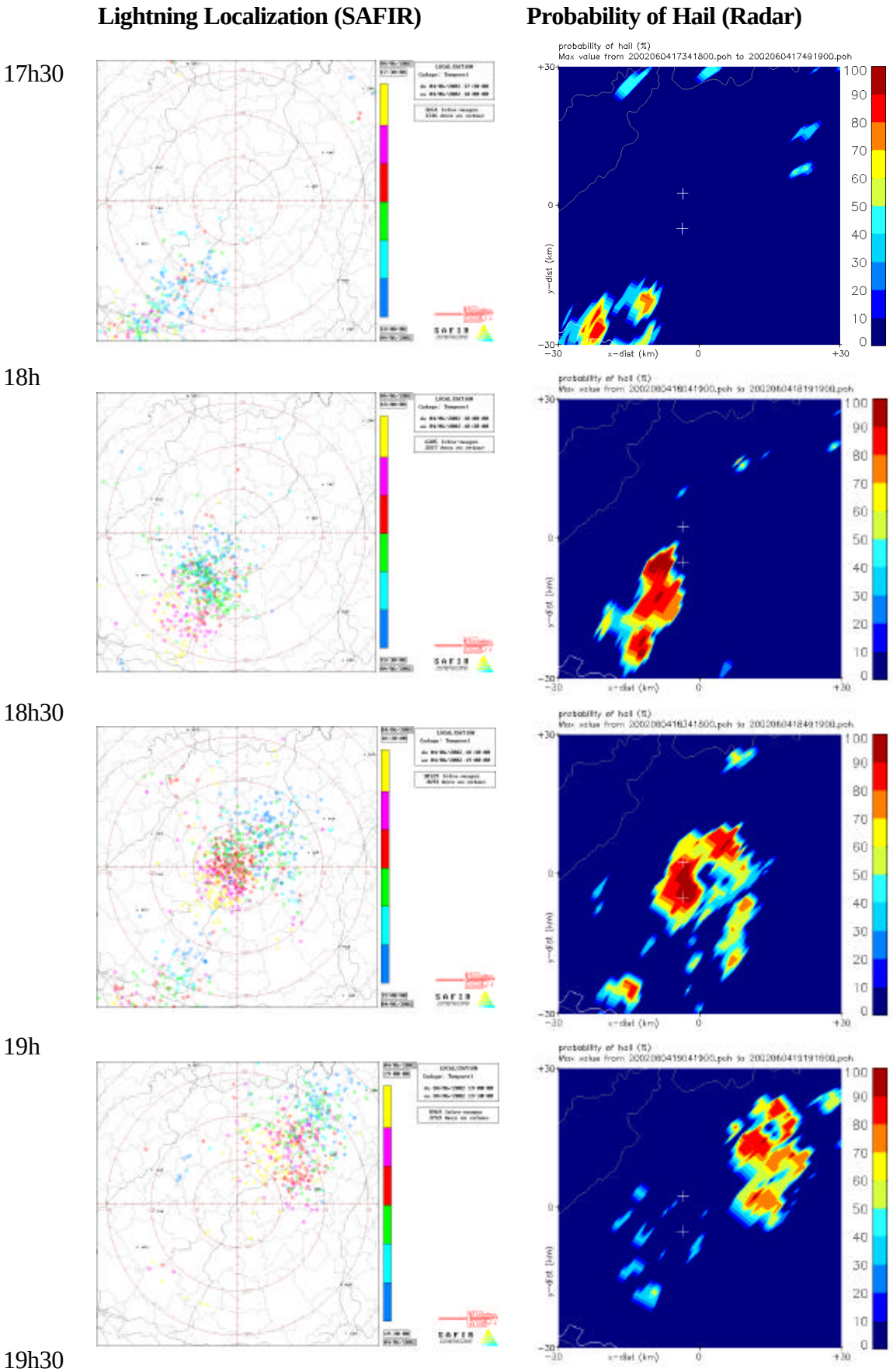

Figure 5.3: Comparison between cloud-to-ground lightning activity and radar-derived probability of hail for the hail event of Lessines on June 4, 2002 (case C1).

6 Mesoscale weather predictions

6.1 Hail forecast from ETA mesoscale model

An explicit hail forecasting method has been recently implemented for routine use at RMI. It is based on the Fawbush-Miller (FM) technique (Miller, 1972; Gordon, 2000) and applied on the output of the mesoscale model ETA (Janjic, 1994; Dehenauw, 2003). This method provides an estimation of the maximum expected size of the hail stones. The present hail case study offers the opportunity to test the method on various hail reported cases.

For the case of April 19 2002, the hail forecasting method does not forecast any hail. This hail episode can not be considered as a typical summer hail case associated with severe thunderstorm. Hail was produced by moderate convection developing in a relatively cold environment. The Fawbush-Miller technique is not designed to predict such kind of hail event. For the five other hail episodes, hail was forecasted. The ETA model is run every 6 hours. For each hail case, the results of the two latest simulations have been considered. The results shown hereafter are those obtained by the simulation predicting the largest hailstones. On each plot, the small crosses indicate the locations of hail reports.

May 26, 2002

The model forecasts hailstones of maximum 1 cm in East and West-Flanders and in the region of Antwerp. Hail was actually reported in these areas (Fig. 6.1). The hailstones in the provinces of Hainaut and Brabant are missed, because there is no precipitation forecast there. The model does not allow hailstone formation in areas where the convective precipitation is zero. However, the model clearly indicates a potential for local hailstones in the observed range of diameters.

June 4, 2002

Hailstones of 2 cm were observed in Lessines. As shown in Fig. 6.2, hail of approximately 2 cm is forecast in the province of Hainaut and Eastern Flanders, very close to Lessines. Hailstones of 3 cm and larger near the border with France could not be confirmed by hail reports.

June 14, 2002

Hailstones up to 2 cm are forecasted and observed for the southwestern part of Belgium in the first part of the evening (Fig. 6.3). Around midnight the model still correctly suggests hail falling on the ground in the central and eastern regions but with overestimation of about 1 cm with respect to the reports (Fig 6.4). However, that does not exclude that locally hailstones could have reached 2 cm diameter.

July 30, 2002

The model's hail forecast area includes the provinces Brabant, Hainaut and Liège, where hailstones were actually observed (Fig. 6.5). The model overestimates the hailstones with 0.5-1 cm.

August 3, 2002

The model indicates potential hail of 1 cm near the locations where hail was observed. We do not have reports of hailstones of 3 cm in the Meuse valley.

In general, the hail forecasting method shows good agreement with ground observations. Nevertheless; some discrepancies are found between the forecasted areas and hailstone diameters and the reported hail cases. In particular, the model seems to overestimate the size of the hailstones. However, it must be kept in mind that a lack of observations does not exclude hail fall in the region. Besides, the large variability of the size of hailstones for a given episode makes also extremely difficult to verify the model-predicted size. In each case, the FM technique applied to the ETA simulations allows a valuable prediction of the risk of hail.

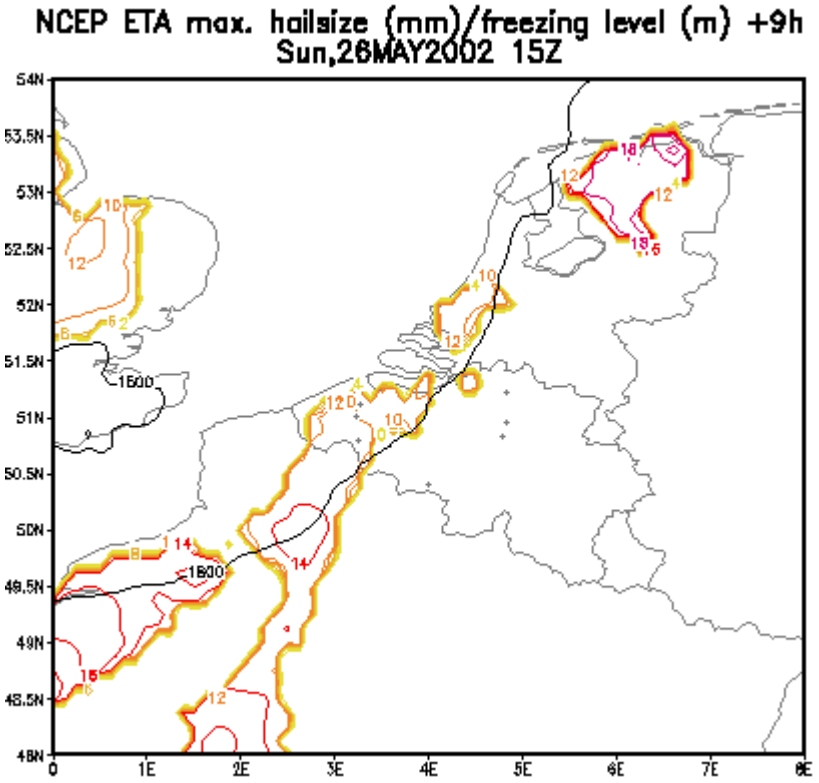

Figure 6.1 : Maximum hail size forecast for May 26 2002 15 UTC (colour isolines) and freezing level height (black isolines). Crosses indicate the locations of the reported hail falls.

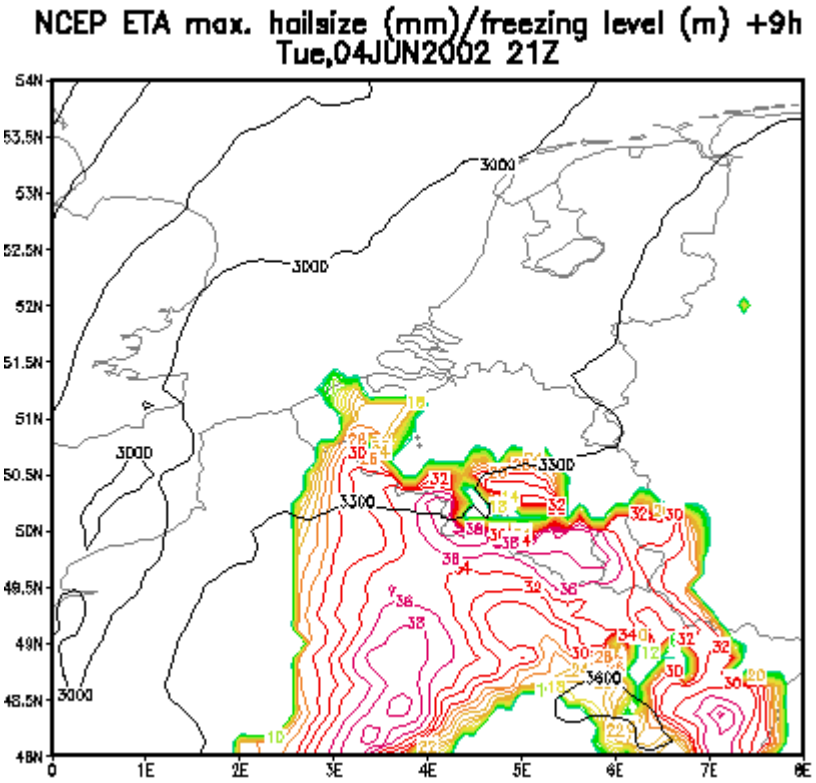

Figure 6.2 : Maximum hail size forecast for June 4 2002 21 UTC (colour isolines) and freezing level height (black isolines). Crosses indicate the locations of the reported hail falls.

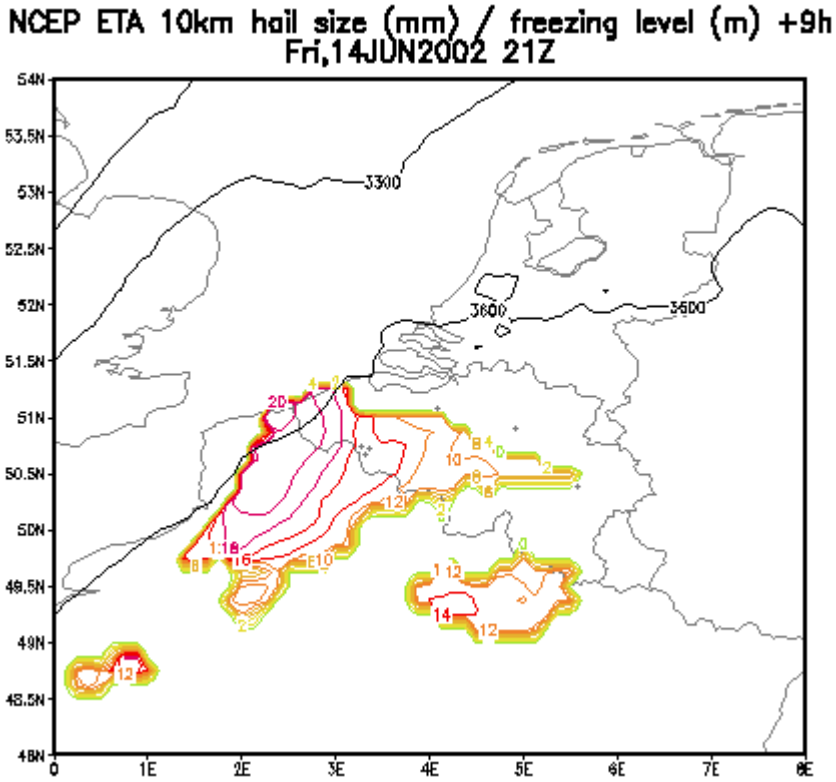

Figure 6.3 : Maximum hail size forecast for June 14 2002 21 UTC (colour isolines) and freezing level height (black isolines) . Crosses indicate the locations of the reported hail falls.

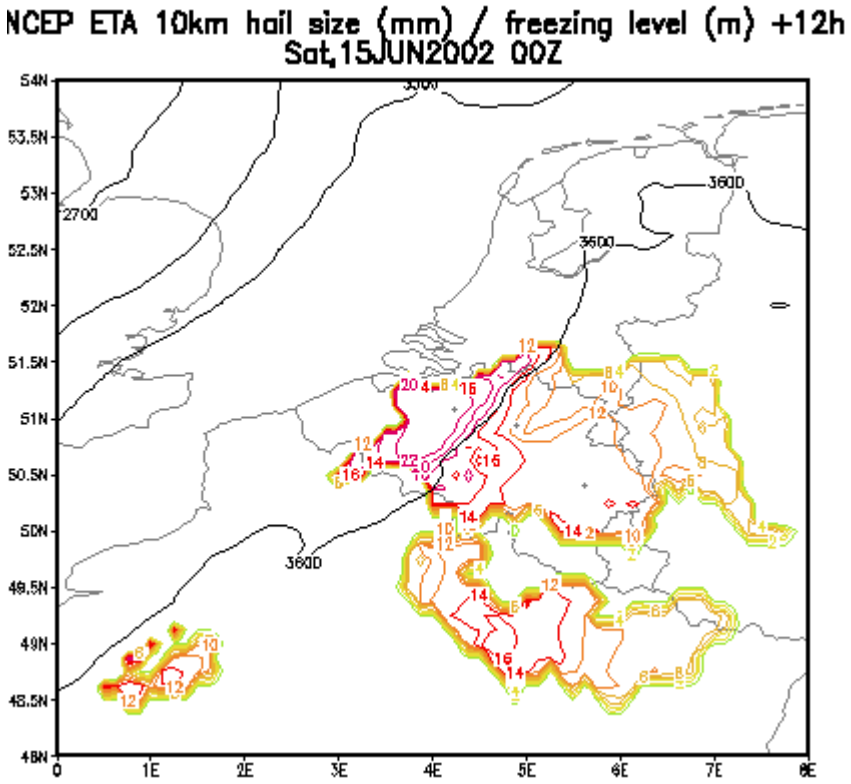

Figure 6.4 : Maximum hail size forecast for June 15 2002 00 UTC (colour isolines) and freezing level height (black isolines). Crosses indicate the locations of the reported hail falls.

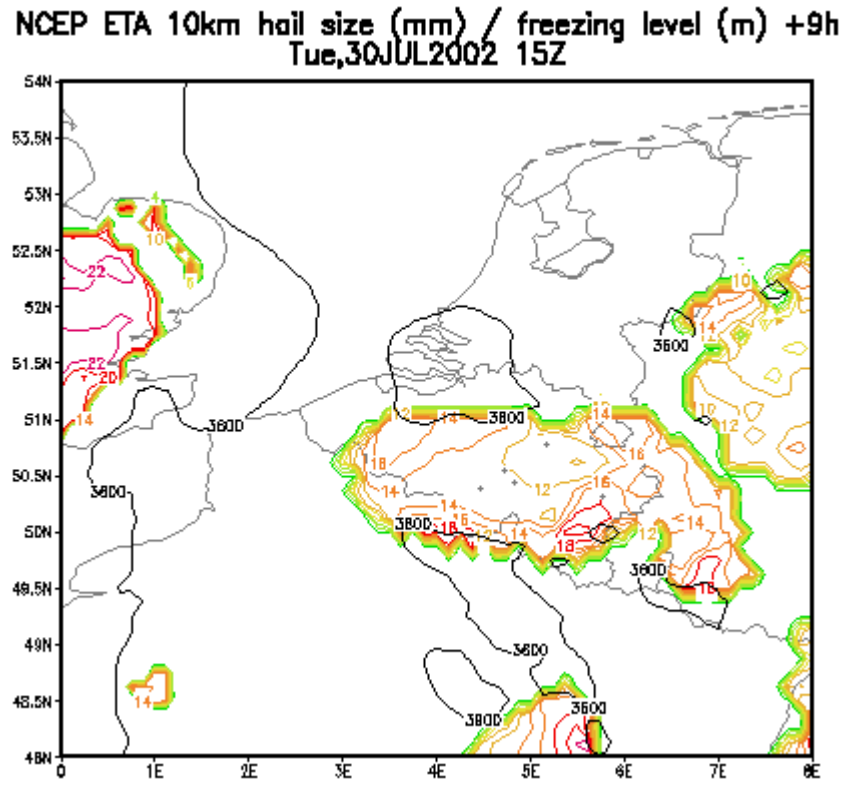

Figure 6.5 : Maximum hail size forecast for July 30 2002 15 UTC (colour isolines) and freezing level height (black isolines). Crosses indicate the locations of the reported hail falls.

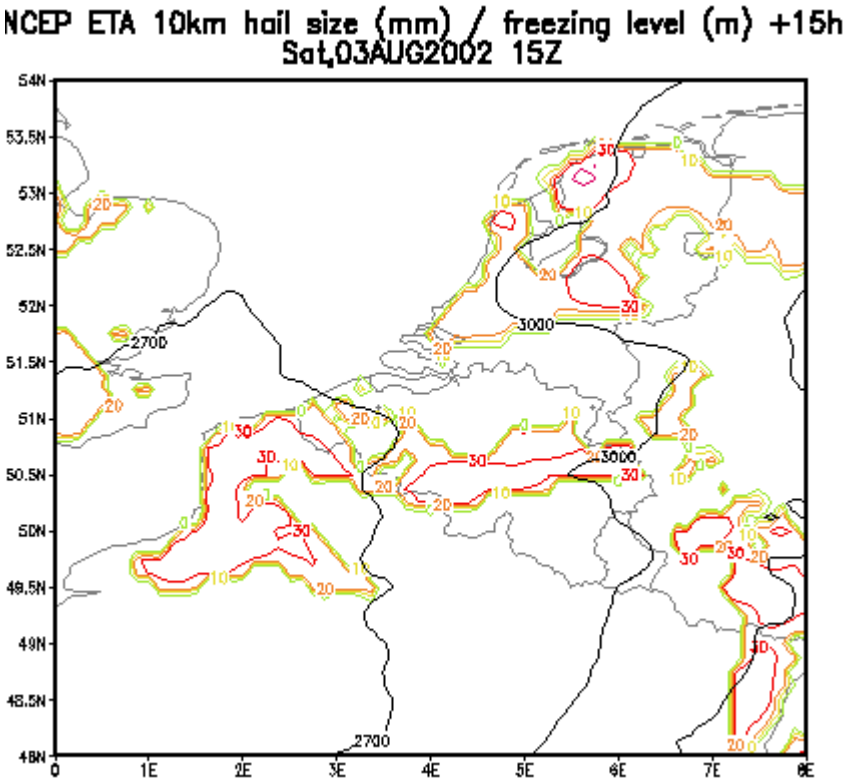

Figure 6.6 : Maximum hail size forecast for August 3 2002 15 UTC(colour isolines) and freezing level height (black isolines) . Crosses indicate the locations of the reported hail falls.

6.2 Contribution of the Aladin Belgium mesoscale model

The high resolution limited area model named Aladin Belgium is a regional forecast model developed by the Royal Meteorological Institute (RMI) and coupled to Aladin France. This model is also supported by a research group at the RMI. It has been run two times per day respectively at 00h00 and 12h00 U.T.C. since march 1998. The model output data are postprocessed to produce a large set of meteorological variables forecasted over a domain of 700 x 700 kilometers centered over Belgium with 41 vertical levels and a grid point resolution of 7 kilometers. The forecast ranges extend up to 48 hours with a time step of 1 or 3 hours.

A few surface and upper-air meteorological fields issued from the model have been selected for the dates of the hail events and are illustrated in the following figures. Up to now no explicit hail forecast indicators have been postprocessed. Nevertheless it appears in the following case studies that the main characteristics of the synoptic and mesoscales patterns favourable to deep convection have been captured in a realistic way by the model.

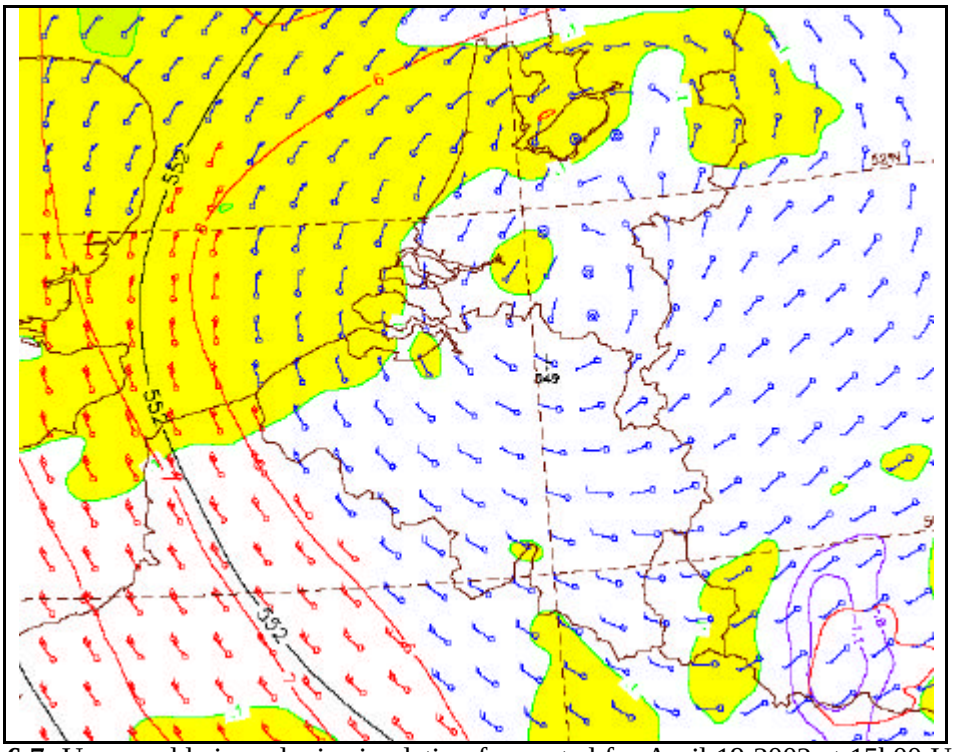

Figure 6.7: Upper cold air cyclonic circulation forecasted for April 19 2002 at 15h00 U.T.C (3-h forecast). The 500 hPa geopotential height (in decameters) and temperature (in degree Celsius) fields are respectively represented by black and red isolines. The grid point winds are described by flags (in knots). The comparison with Fig. 3.1 shows that the cold air depression is properly captured by the model.

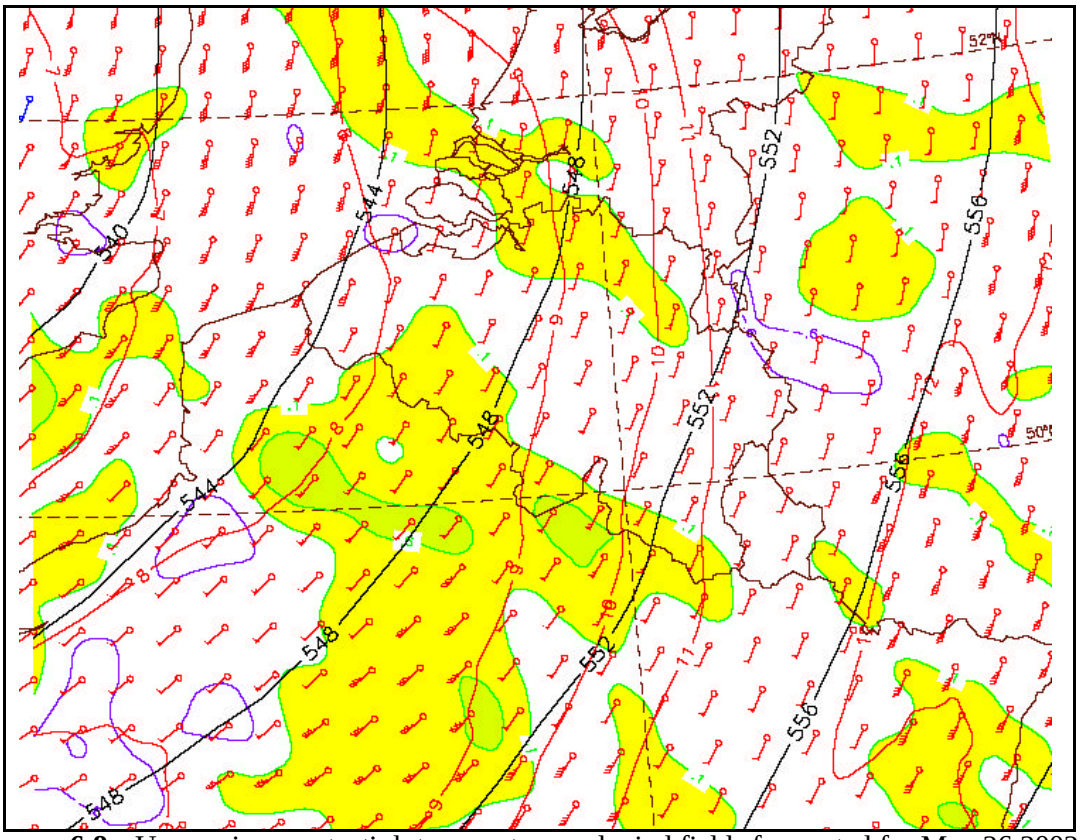

Figure 6.8 : Upper-air geopotential, temperature and wind fields forecasted for May 26 2002 at 12h00 U.T.C (12-h forecast). The 500 hPa fields are represented as in Fig. 6.7. These upper-air fields indicate that the dynamic upper trough analysed in Fig. 3.2 is well depicted.

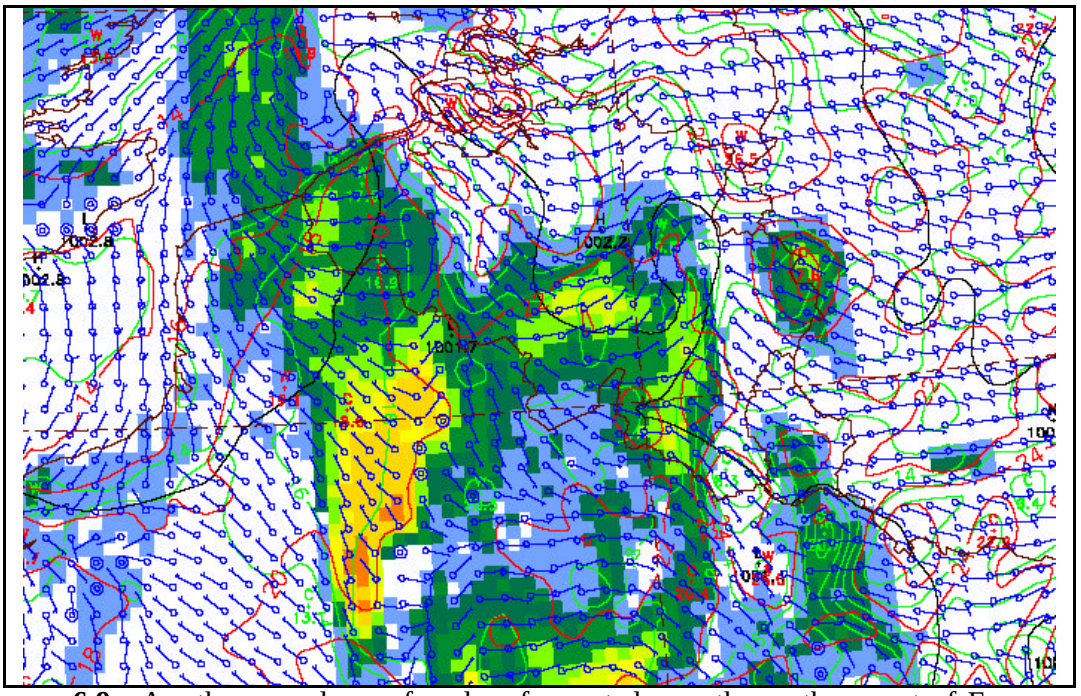

Figure 6.9 : A rather complex surface low forecasted over the northern part of France and Belgium in the evening of June 4 2002 at 18h00 U.T.C (18-h forecast). The 3-hour cumulated precipitation is represented by coloured areas and the grid point surface wind by flags (in knots). As in Fig. 3.3 a sharp mesoscale convergence line extends from northern France to the western part of Belgium and the North sea.

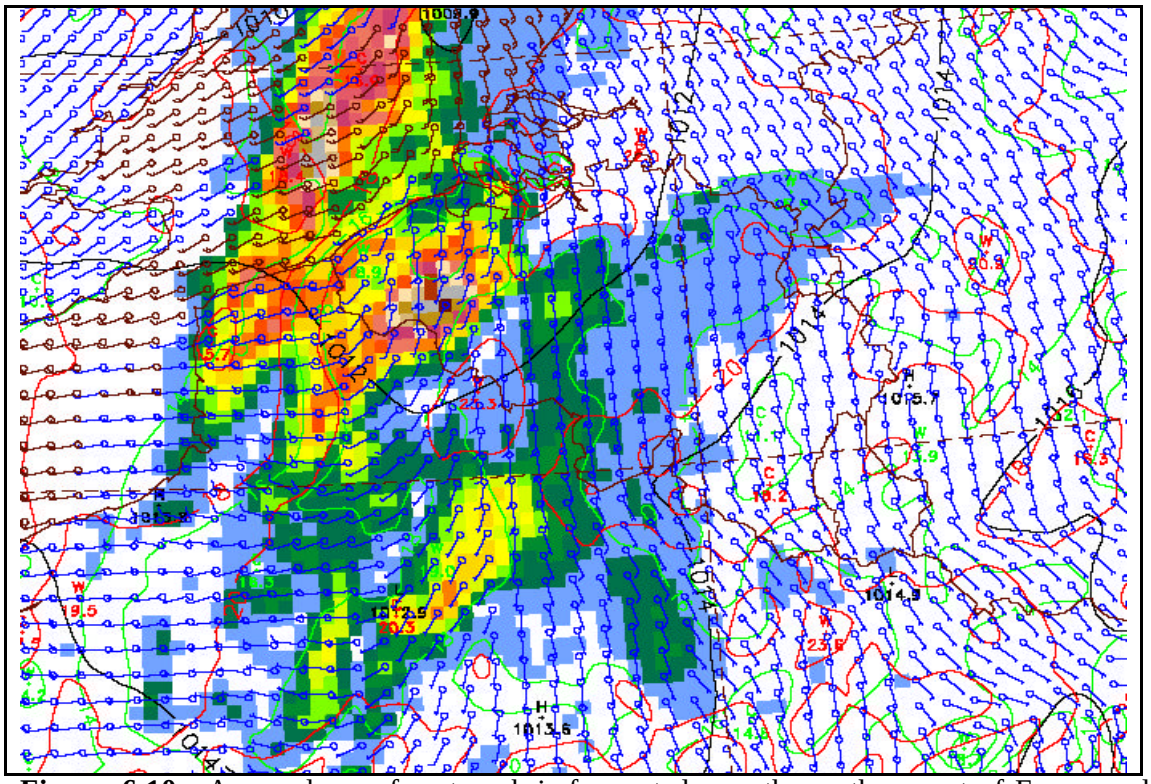

Figure 6.10 : A complex surface trough is forecasted over the northern part of France and Belgium, late in the evening (at 21.00 U.T.C.) of June 14 2002 (18-h forecast). The 3-hour cumulated precipitation and the surface winds are represented in the same way as in Fig. 6.9. A sharp convergence line associated with the surface trough is forecasted in a realistic way over the north of France and the west part of Belgium.

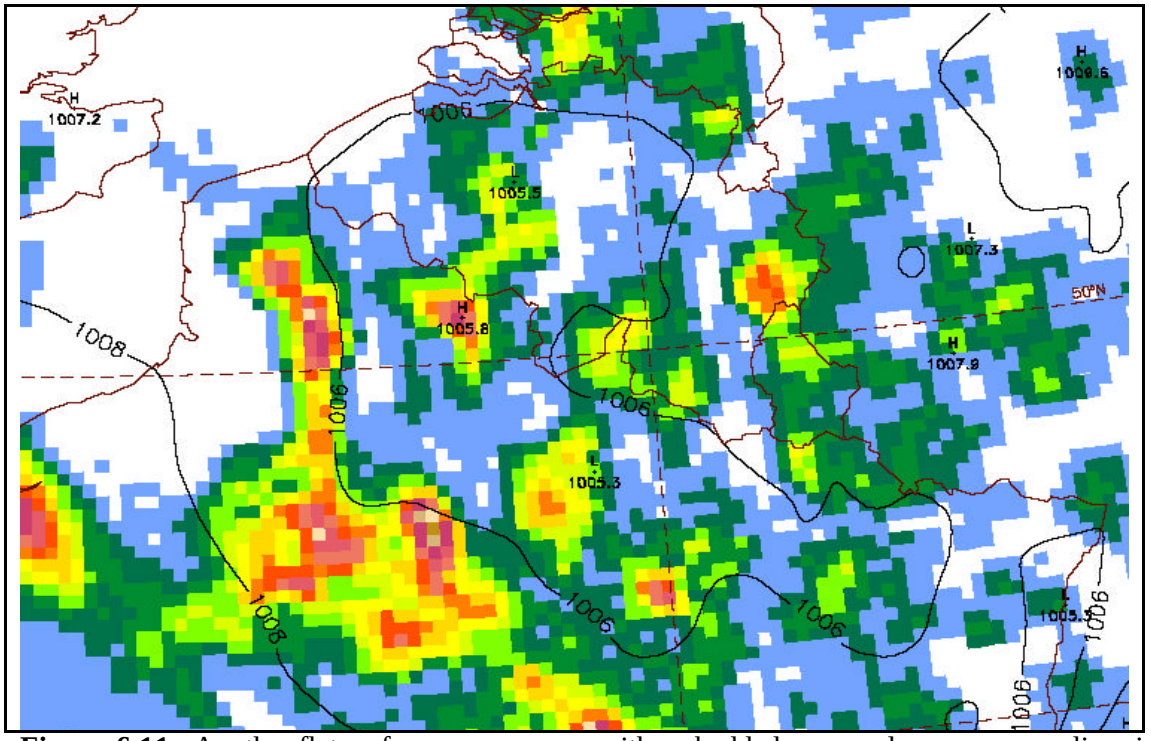

Figure 6.11 : A rather flat surface pressure area with embedded mesoscale convergence lines is forecasted during the afternoon for July 30 2002 at 18 U.T.C (18-h forecast). The 3-hour cumulated precipitation (coloured areas) indicate a high probability of convective precipitation over our areas except over the North sea and the close coastal areas.

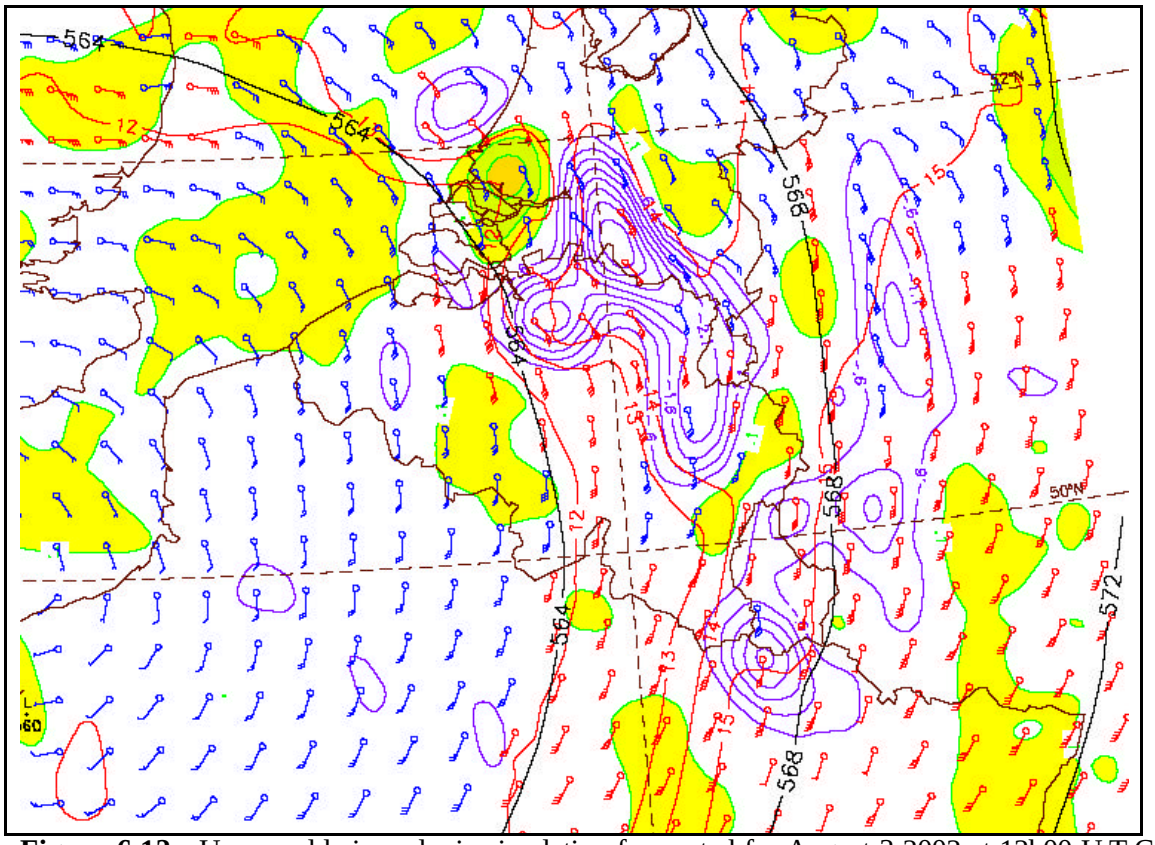

Figure 6.12 : Upper cold air cyclonic circulation forecasted for August 3 2002 at 12h00 U.T.C (12-h forecast). The 500 hPa geopotential height, temperature and wind fields are described as in Fig. 6.7. The comparison with Fig. 3.6 shows that the cold air depression is properly depicted by the model.

7 Conclusions

The aim of this study was to test a radar-based hail detection algorithm and to analyse various hail episodes using different observational and forecasting tools. Based on hail reports collected from the RMI network of observers, 23 hail cases have been selected with precise information on time, location, and size of the hail stones.

Among various methods proposed in the literature, the method of Waldvogel (1979) has been selected to derive the probability of hail from the volumic reflectivity data collected by the radar of Wideumont. The probability of hail is determined as a function of the height difference between the freezing level and the maximum height where a reflectivity at least equal to 45 dBZ is measured. The formulation has been adjusted by Holleman (2001) based on an extensive verification study carried out in The Netherlands.

The selected hail detection method has been implemented and tested on the different reported hail cases. For 22 cases on 23, a probability of hail at least equal to 50 % was found at less than 10 km from the reported location of hail fall. For 16 cases on 23, a probability of hail at least equal to 70 % is found. Hail cases with larger hail stones are detected with a higher probability of hail. Even if these results are based on a relatively small number of hail cases, it suggests that the method is able to detect most hail events. It should be noted that the present study does not allow an evaluation of the probability of false alarm. Most hail falls are not reported which makes the estimation of false alarm rate extremely difficult.

The meteorological situations associated with hail storms have been analysed. For the episodes of the summer 2002, hail thunderstorms were associated either with upper cold air lows, dynamical upper troughs or mesoscale convergence lines associated with thermal troughs.

For the different hail cases, data from the lightning detection system SAFIR have been collected in order to investigate the relation between the electrical activity and the probability of hail derived from radar data. A very good agreement has been found between the location of the areas of high electrical activity and the areas of high probability of hail. Furthermore, hail cases with larger reported size of hailstones are associated with higher electrical activity.

The contribution of the operational model ALADIN Belgium developed at RMI has been evaluated for the reported hail cases. It relies on several surface and upper air fields mostly at mesoscales. In most cases, the conditions favourable to deep convection are correctly simulated by the model . The timing and the localization of the convective conditions are generally well predicted but a reliable forecast of the degree of severity appears more difficult.

The performances of a hail forecasting method recently implemented at RMI have also been evaluated for the reported hail cases. It is based on the Fawbush-Miller technique and applied to the output of the ETA mesoscale model. In almost all cases, hail is correctly forecasted over Belgium. Nevertheless, the location of hail is not always well predicted by the model. Due to the sporadic nature of hail thunderstorms and the

difficulties in explicit and detailed convection forecasts, a reliable prediction of the affected areas remains a challenge.

The results obtained in the present study are very encouraging. We have shown the benefit gained by the combined use of different observational and forecasting tools. As far as radar-based hail detection is concerned, the tested method has shown good performances on the selected hail cases. Based on these results, it seems appropriate to implement this method at the Weather Office and to further test it in semi-operational conditions. This will allow to evaluate the performances of the hail detection method on a large number of hail episodes. Besides, the hail detection product will provide valuable information to the Climatological Service for the a-posteriori assessment of reported hail events.

Acknowledgments

The assistance of many collaborators was greatly appreciated by the authors. We want to acknowledge the contribution of the observers of the climatological network and weather amateurs for the collection of hail reports. We are grateful to Luc Debontridder and Alex Dewalque of the Climatological Service who provided assistance in the treatment of these reports. The support of colleagues from the Weather Office for the meteorological analysis was highly appreciated. We are particularly grateful to Geert De Sadelaer, Christophe Ferauge and Michel Crabbé. By ensuring the good working of the radar and SAFIR systems, they provided an essential contribution to this work. Constructive remarks made by Dirk De Muer, Edward De Dycker, and Christian Tricot on a first version of this report were greatly appreciated. Finally, we want to thank our colleague Iwan Holleman from the Netherlands Royal Meteorological Institute. His experience on the use of radar data for hail detection in The Netherlands was of great benefit for the present study.

References

Amburn, S.A., and P.L. Wolf, 1997. VIL density as a hail indicator. Wea. and Forecasting, 12, 473-478.

Atlas, D., and F.H. Ludlam, 1961. Multi-wavelength radar reflectivity of hail storms. Quart. J. Roy. Meteor. Soc., 87, 523-534.

Auer, A.H. Jr, 1994. Hail recognition through the combined use of radar reflectivity and cloud-top temperatures. Mon. Wea. Rev., 122, 2218-2221.

Bergeron, 1933. On the physics of clouds and precipitation. Proc. Fifth. Assembly U.G.G.I. , Lisbon, 156-178.

Böhm, J.P., 1989. A general equation for the terminal fall speed of solid hydrometeors. J. Atmos. Science, 46, 2419-2427.

Browning, K.A., and G.B. Foote, 1976. Airflow and hail growth in supercell storms and some implication for hail suppression, Quart. J. R. Met. Soc., 102, 499-533.

Crum, T.D., and R.L. Alberty, 1993. The WSR-88D and the WSR-88D Operational Support Facility. Bull. Amer. Meteor. Soc., 74, 1669-1687.

Dehenauw, D., 2003. An objective hail size forecasting method based on mesoscale model output, Scientific publication, Royal Meteorological Institute of Belgium, 2003.

Delobbe, L. and I. Holleman, 2003. Radar-based hail detection: impact of height assignment errors on the measured vertical profiles of reflectivity. Preprints, 31st Intenational Conference on Radar Meteorology, Seattle, U.S.A, Amer. Meteor. Soc., 475-478.

Feral, L., H. Sauvageot, and S. Soula, 2003. Hail detection using S- and C- band radar reflectivity difference, J. Atmos. Oceanic Technol., 20, 233-248.

Gordon, J.D., 2000. A comprehensive severe weather forecast checklist and reference guide. NOAA Technical Service publications NWS CR-10.

Greene, D.R., and R.A. Clark, 1972. Vertically integrated liquid water – a new analysis tool. Mon. Wea. Rev., 100, 548-552.

Heymsfield, H., A.R., Jameson, and H.W. Frank, 1980. Hail growth mechanisms in a Colorado Storm : part II : hail formation processes, 37, 1779-1807.

Holleman, I., 2001. Hail detection using single-polarization radar. Scientific report 2001/01, Royal Netherlands Meteorological Institute (KNMI).

Jameson, A.R., and Johnson, D.B., 1990. Convective Dynamics. D. Atlas (Ed.), Radar in Meteorology, Amer. Meteor. Society, 323-347.

Janjic, Z.I., 1994. The step-mountain eta coordinate model : Further developments of the convection, viscous sublayer and turbulence closure schemes, Mon.Wea.Rev., 122, 927-45

Kessinger, C.J., E.A. Brandes, and J.W. Smith, 1995. A comparison of the NEXRAD and NSSL hail detection algorithms. Preprints, 27th Conf. on Radar Meteorology, Vail., CO, Amer. Meteor. Soc., 603-605.

Mason, B.J., 1971. The physics of clouds. Clarendon Press, Oxford, UK.

Miller, R.C., 1972. Notes on analysis and severe storm forecasting procedures of the Air Force Global Weather Center. AWS Technical report 200 (Rev), Headquarters, Air Weather Service, Scott AFB, IL, 106 pp.

Nelson, 1983. The influences of storm flow structure on hail growth. J. Atmos. Sci., 40, 1965-1983.

Pruppacher, H.R., and Klett, J.D., 1997. Microphysics of Clouds and Precipitation. 2nd Edition, Dordrecht, Kluwer Academic Publishers.

Ray, P., 1990. Convective Dynamics. D. Atlas (Ed.), Radar in Meteorology, Amer. Meteor. Society, 348-390.

Seliga, T.A., K. Aydin, C.P. Cato, and V.N Bringi, 1982. Use of the differential reflectivity radar technique for observing convective systems. Cloud dynamics, E.M. Agee and T. Asai (Eds.), Reidel, 285-300.

Smart, J.R., and R.L. Alberty, 1985. The NEXRAD hail algorithm applied to Colorado thunderstorms. Preprints, 14th Conf. on Severe Local Storms, Indianapolis, IN, Amer. Meteor. Soc., 244-247.

Waldvogel, A., B. Federer, and P. Grimm, 1979. Criteria for the detection of hail cells. *J. Appl. Meteor.*, **18**, 1521-1525.

Witt, A., M.D., Eilts, G.J. Stumpf, J.T. Johnson, E. D. Mitchell, and K.W. Thomas, 1998. An enhanced hail detection algorithm for the WSR-88D. Wea. and Forecasting, **13**, 286-303.